Improving agricultural efficiency with solar-powered tractors and magnetohydrodynamic entropy generation in copper–silver nanofluid flow

10 authors, including:

Adebowale Martins Obalalu
Augustine university
53 PUBLICATIONS   519 CITATIONS

Mohanad Alqarni
Albaha University
27 PUBLICATIONS   171 CITATIONS

Muhammad Asif Memon
Sukkur Institute of Business Administration
37 PUBLICATIONS   102 CITATIONS

Olalekan Olayemi
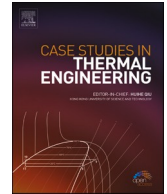Kwara State University, Ilorin, Nigeria
40 PUBLICATIONS   172 CITATIONS

Improving agricultural efficiency with solar-powered tractors and magnetohydrodynamic entropy generation in copper–silver nanofluid flow

A.M. Obalalu [a], M.M. Alqarni [b], C. Odetunde [c], M. Asif Memon [d], O.A. Olayemi [e,f], A.B. Shobo [g], Emad E. Mahmoud [h], Mohamed R. Ali [i,j,*], R. Sadat [k], A.S. Hendy [l]

[a] Department of Mathematical Sciences, Augustine University Ilara-Epe, Lagos, Nigeria
[b] Department of Mathematics, College of Sciences, King Khalid University, Abha, 61413, Saudi Arabia
[c] Faculty of Engineering, Augustine University Ilara-Epe, Lagos, Nigeria
[d] Department of Mathematics and Social Sciences, Sukkur IBA University, Sukkur, 65200, Sindh, Pakistan
[e] School of Engineering, Cranfield University, Cranfield, UK
[f] Department of Aeronautics and Astronautics, Kwara State University, Malete, 23431, Nigeria
[g] Departamento de Ingeniería Mecánica, Universitat Rovira i Virgili, Carretera de Valls, 43007, Tarragona, Spain
[h] Department of Mathematics and Statistics, College of Science, Taif University, PO Box 11099, Taif, 21944, Saudi Arabia
[i] Faculty of Engineering and Technology, Future University in Egypt, New Cairo, 11835, Egypt
[j] Basic Engineering Science Department, Benha Faculty of Engineering, Benha University, Benha 13518, Egypt
[k] Department of Mathematics, Zagazig Faculty of Engineering, Zagazig University, Egypt
[l] Department of Computational Mathematics and Computer Science, Institute of Natural Sciences and Mathematics, Ural Federal University, 19 Mira St., Yekaterinburg, 620002, Russia

ARTICLE INFO

ABSTRACT

This study examines the impact of solar-powered tractor on agricultural productivity and energy efficiency. The implementation of solar energy in tractors has the potential to reduce dependence on non-renewable energy sources, minimize carbon emissions, and promote sustainable farming practices. This research investigates the reduction of energy consumption and enhancement of productivity by evaluating magnetohydrodynamic (MHD) entropy production through the flow of nanofluids containing copper-engine oil (Cu-EO) and silver-engine oil (Ag-EO). The study also evaluates the effectiveness of thermal transport in solar-powered tractors through several properties such as solar thermal radiation, viscous dissipation, slippery velocity, and porous media. The investigation analyzed the thermodynamics of entropy generation in a non-Newtonian Williamson nanofluid, with the aim of assessing its energy equilibrium and the effects of diverse physical parameters. In order to enable numerical investigation, similarity variables were implemented to transform partial differential equations into ordinary differential equations, and the Chebyshev collocation spectral method was applied to solve the governing equations. It has been revealed that the $Ag - EO$ Williamson nanofluid have a smoother flow compared to the $Cu - EO$ mixture fluid. Furthermore, Williamson-nanofluid demonstrate superior thermal conductivity and heat transfer characteristics compared to the base fluid, making them appropriate for utilization in cooling systems and heat exchangers in various industries. The boundary layer exhibits

the maximum temperature while employing lamina-shaped particles, whilst the lowest temperature is shown when utilizing spherical-shaped nanoparticles. The Ag-EO nanofluid an efficiency rate of approximately 2.64 % with a minimum efficiency rate of 3.22 %. The findings will help develop eco-friendly agricultural methods that promote economic development while mitigating harm to the environment.

Nomenclature

R_1	Velocity component in x-direction (unit: m/s)
R_2	Velocity component in y-direction (unit: m/s)
T_w	Temperature at the surface of the wall(unit:K)
μ_{nf}	Dynamic viscosity
ρ	Fluid density (unit: kgm^{-3})
k_{hnf}	Thermal conductance
R_w	porosity of the encompassing plate
N_x	Slip length (unit: m)
Ω	dimensionless temperature (unit:K)
Br	Brinkman number
ζ	Williamson fluid
B_i	Biot number
φ	volume friction of nanoparticles
C_P	Specific heat capacity (unit: mol Jk $g^{-1}K^{-1}$)
ψ	Stream function (unit: $\frac{Kg}{m}.s$)
ρ	Fluid density (unit: kgm^{-3})
T_∞	ambient temperature (unit:K)
k_0	thermal conductivity of solid
t	Time (unit:s)
$(\rho C_p)_{nf}$	specific heat
σ_{nf}	electric conductivity
h_f	heat transfer coefficient
Re	Reynolds number
K_N	permeability parameter
R_N	thermal radiation
Ec	Eckert number

1. Introduction

Heat transmission (HT) is a field of heat research that focuses on the production, utilization, modification, and preservation of thermal energy systems. In recent years, there has been an increased interest in the field of HT due to the growing concern over climate change and its impacts on energy systems. As the world seeks to reduce its carbon footprint and transition towards renewable energy sources, understanding the principles of HT has become more critical than ever before. This article aims to provide an overview of the fundamentals of HT, its applications, and its importance in the context of renewable energy and climate change. The study of HT is comprised of various components, including the transfer of heat through conduction, convection, and radiation [1]. Many researchers propose various methods of explaining heat transfer concepts in engineering problems [2,3]. Some of the applications investigated include spaceship design, comets and asteroids, mass transfer preservation, heat exchanger design, and heat piping system development.

In recent years, the amount of carbon dioxide entering the atmosphere as a result of various industrial activities has markedly increased. The main origin of greenhouse gas emissions that result in climate change and air pollution is the utilization of energy, which encompasses carbon dioxide (CO_2) [4]. Moreover, the escalation of CO_2 levels in the atmosphere plays a significant role in the acceleration of global warming and climate change, which can have far-reaching consequences on human health and overall well-being. Also, the combustion of coal, oil, and natural gas for electricity generation, transportation, and heating processes releases significant amounts of CO_2 into the atmosphere. The pollution and high levels of atmospheric CO_2 are dangerous to all living organisms on Earth, we must find ways to reduce the number of CO_2 emissions. By utilizing solar energy, we can undoubtedly alleviate the harmful effects of CO_2 emissions by decreasing the total quantity of carbon dioxide discharged into the atmosphere. According to the projections made by the Intergovernmental Panel on Climate Change (IPCC), solar energy is the singular energy source that possesses both environmental friendliness and long-term sustainability. Solar power is a clean and renewable form of energy that comes from the sun's rays. It can be transformed into electricity or heat without releasing any harmful emissions, making it environmentally friendly.

The primary method of harnessing solar energy is through the use of solar panels composed of photovoltaic cells that trap sunlight and transform it into useable energy. The utilization of solar energy provides numerous environmental benefits, including its renewability and sustainability, ability to reduce the environmental impact, conserve water resources, decrease air pollution, and lower greenhouse gas emissions. The researched by of Jahangir et al. [5] utilized the hybrid renewable energy systems to minimize the number of carbon emissions produced by large industrial livestock farms. The recent work of Aziz et al. [6] examine the correlation between carbon pricing and environmental degradation, particularly highlighting the significance of the demand for solar energy as a contributing factor to this relationship. A modeling approach proposed by Ref. [7] investigates the impacts of climate change on the usage of renewable energy.

The transportation sector constitutes a noteworthy contributor to global greenhouse gas emissions, accounting for approximately 27 % of such emissions [8]. This phenomenon is primarily attributed to the utilization of fossil fuels, namely gasoline and diesel, for transportation purposes. The combustion of these fuels generates carbon dioxide and other greenhouse gases that have the capacity to trap heat in the atmosphere, thereby contributing to global warming. Over the past few years, there have been notable developments in utilizing solar energy for transportation. Solar energy represents a sustainable and easily accessible source of power, which can be utilized to effectively propel various modes of transportation including automobiles, watercraft, airplanes, and trains. Developments in this domain have resulted in the creation of solar-powered tractors, trains, boats and yachts, airplanes, as well as other types of vehicles.

The use of the solar-powered tractor and hybrid-electric tractors is becoming increasingly popular in the agriculture sector. These types of tractors utilize both solar power and electricity to minimize fuel usage and lower greenhouse gas emissions, and also enhance effectiveness and output. Usually, a tractor that runs on solar energy has a set of solar panels fixed on its roof or other external areas. These panels transform sunlight into electrical energy, which can be utilized to run the tractor's electric motor or other devices such as GPS, fans, or lights. In contrast, hybrid-electric tractors utilize both a conventional gasoline or diesel engine and an electric motor to propel the vehicle [9]. They are typically equipped with regenerative braking mechanisms that harness the energy that would otherwise be wasted during braking and repurpose it to recharge the batteries or supply power to other systems. Using solar-powered or hybrid-electric tractors offers several advantages such as cost savings on fuel, reduced emissions, and increased efficiency. Additionally, these tractors operate quietly compared to traditional tractors which can be useful in settings like residential or urban areas. Using tractors that are powered by solar or hybrid-electric energy sources presents some difficulties such as the initial expenses involved and the requirement of adequate sunlight or battery power to run the vehicle over prolonged periods. Nevertheless, advancements in solar and battery technology may alleviate these concerns, making this an increasingly viable and accessible option in the future. Farm machineries such as tractors run on diesel fuel which can contribute to various forms of pollution including global warming, air pollution, and contamination of the soil and groundwater in case of spills. The tractor, a small truck, is energized by a 12 KW electric motor and requires 16 lead batteries to function. This setup includes a collection of photovoltaic modules that generate sustainable energy, a battery-powered tractor with multiple applications, and the ability to power up to a 40-horsepower light bulb, as well as an energy-saving battery system. During the 1970s and 1980s, Heckeroth, the inventor of the solar tractor, devoted his efforts to developing a blueprint for solar residences and sustainable energy commodities. Later on in the 1990s, they began introducing electric vehicles. The rapid progression of agricultural technology is advancing at a swift pace. The alterations made are aimed at enhancing the productivity of farms in terms of equipment, machinery, and resources [10]. The use of nanofluid has significantly improved the thermal conductivity of solar-powered tractors, thereby boosting their efficiency in agricultural operations involving both plants and animals. The researcher conducted by Ref. [11], examined the thermal efficiency of a time-varying nanofluid with magneto properties flowing through a solar-powered tractor. The study used Keller box analysis and incorporated a factor for the shape of the nanometal. In an article referenced as [12], the topic of discussion is the impact of solar-powered electrical equipment on the promotion of sustainable farming practices. The authors contend that the incorporation of solar power can contribute to a reduction in greenhouse gas emissions and facilitate energy self-sufficiency for farmers. The article emphasizes the advantages of solar-powered machinery for small-scale farmers who may face constraints in accessing conventional energy sources. A solar-powered electric tractor was developed by researchers for agricultural purposes, as reported in a related study [13]. The authors described the tractor's design and development, highlighting its use of a lithium-ion battery and a 5 kW electric motor. The tractor underwent testing in a range of agricultural scenarios, with positive findings regarding its efficiency and performance. The recent work of [14] explores the proper sizing of powertrain components for battery electric tractors, which involves analyzing energy consumption and driving patterns. The authors conducted an assessment of performance using a traction motor and investigated the effects of vehicle weight, tire size, and operating conditions. This research could have significant consequences for the advancement of environmentally friendly and resource-efficient agricultural equipment.

Magnetohydrodynamics (MHD) explores the behavior of fluids capable of conducting electric currents, such as plasma, liquid metals, or saltwater, in the presence of magnetic fields. This interdisciplinary field integrates the principles of fluid mechanics and electromagnetism to provide insight into the dynamics of such fluids [15,16]. The practical application of MHD technology for solar energy generation presents a range of challenges. These include the need for strong magnetic fields, difficulties in controlling plasma and fluid flow, and high operating temperatures, which arise when utilizing MHD generators or wind turbines. In the case of MHD wind turbines, their effectiveness is constrained by the relatively low power density of wind. The field of solar energy could experience a significant transformation with the help of Magnetohydrodynamics. This technology can efficiently convert solar energy into electricity by utilizing MHD generators that transform the kinetic energy of moving fluids like seawater or liquid metal into electrical energy through interaction with a magnetic field. MHD has the potential to tap into underutilized renewable energy sources from ocean currents, tides, and waves. Additionally, MHD wind turbines could offer a more efficient way to generate electricity from wind power. Through further research and development, Magnetohydrodynamics could become an essential tool to meet global energy

demands while reducing greenhouse gas emissions. MHD pertains to studying the conduct of small liquid formations, such as heating or cooling mechanisms, that are useful in diverse industries, engineering, and technological courses. The work of [17] study employs a mathematical model that takes into consideration a range of elements, such as magnetohydrodynamic Maxwell nanofluid, slip circumstances, thermal radiation, and fluctuating thermal conductivity, to examine the heating of solar collectors. The investigation by Ref. [18] employed a method that targeted the reduction of disorder to enhance the arrangement of a fluid flow that involves both convective and magnetohydrodynamic forces within a vertical channel. This channel is subject to the influence of thermal radiation and slip boundary conditions.

A tractor powered by solar energy shows positive impacts on the environment and finances. It runs on a battery that is controlled by a computer and does not require a radiator. The machine operates quietly, making it pleasant to use due to its noiseless performance. The device can operate for 5–8 h on a single battery charge. It is available at the same price as a diesel tractor and does not require any additional expenses. One downside of this tractor is that it doesn't require any maintenance, but this also means there are no additional costs involved. Sustainable agriculture greatly relies on the significant technological progress made by the agricultural industry, which is essential to enhancing the value of agricultural products and satisfying the energy requirements for irrigation and machinery operations. Some of the progress made includes improved farming techniques, the establishment of agro-processing facilities, and the management of solar power stations and irrigation systems. Moreover, the development of innovative equipment and intelligent climate solutions has resulted in a decrease in carbon emissions and effectively tackled the continuously rising fuel expenses and increasing temperature requirements. Solar-powered water pumps and farming equipment that rely on photovoltaic technology are popular components of a solar system in agriculture. Fig. 1 displays the prototype of current theoretical research that follows a symmetrical flow.

Nanofluids are liquids that incorporate nanoparticles; these fluids can be utilized with a solar collector that is shaped like a parabolic trough. Nanofluids have enhanced thermal conductivity and heat transfer rates, which make them a good option to be employed in solar thermal systems. These qualities make nanofluids interesting for application in solar thermal systems. Another kind of solar thermal technology is known as a parabolic trough solar collector. This system makes utilizes a mirror in the shape of a parabolic reflector to collect light onto an absorber tube that is positioned at the focus of the parabolic reflector. The concentrated sunlight gets absorbed by a heat transfer fluid within the absorber tube, which causes the fluid to heat up. Since the mirror is parabolic in shape, it can monitor the sun's movement all day and direct its rays directly onto the receiving tube. The heated fluid can be used directly for heating or other industrial uses, or it can be used to generate power using a steam turbine. In large-scale solar power facilities, where many solar collectors are connected in lines to absorb and concentrate sunlight, which are the most common type of
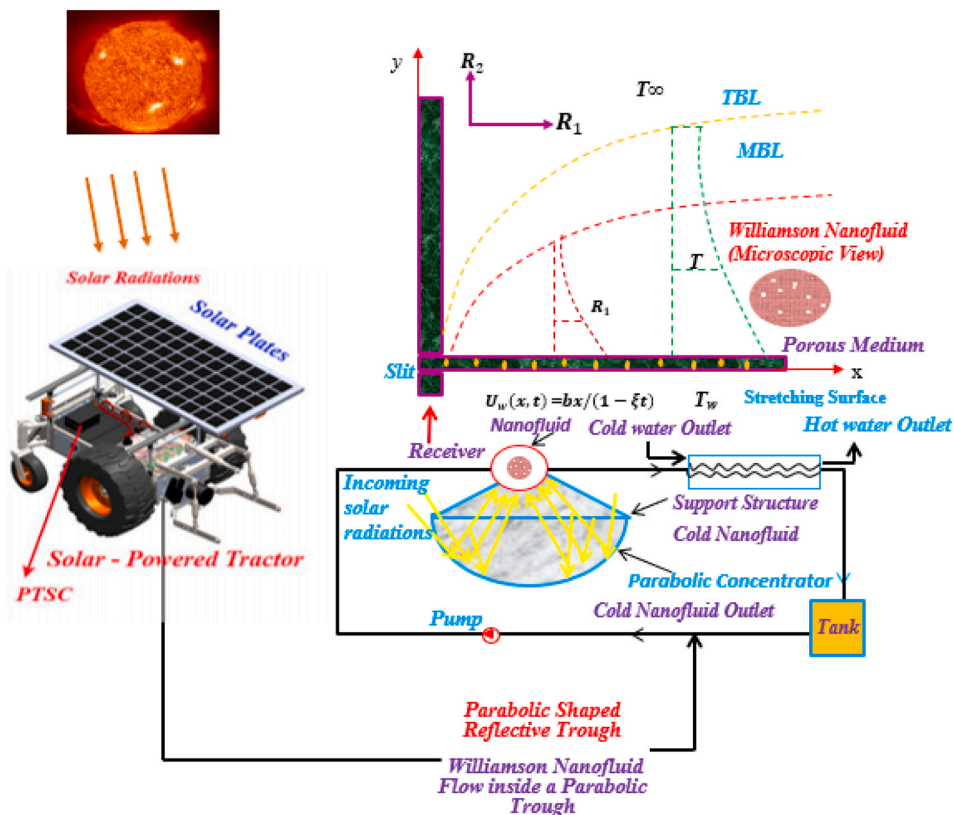

Fig. 1. Diagram representation of the present theoretical model.

solar collector to be utilized is the parabolic trough solar collector (PTSC). It is generally regarded as among the most developed and easily obtainable solar thermal technologies due to their shown histories of dependability and effectiveness in different applications. It is necessary to install a parabolic trough solar collector on a solar-powered tractor, but doing so would demand a substantial quantity of modification and adjustment. A parabolic trough solar collector on a solar power tractor could be utilized to supply extra power for recharging the tractor's batteries or for operating secondary machinery such as sprayers or irrigation pumps, as possible use case [19]. Similarly, there have been accounts of the use of NF as a functional liquid in PTSC from both experimental and computational studies.

Salawu et al. [20] this study focuses on the flow rate, thermal distribution and entropy generation of the magnetized hybrid Prandtl–Eyring nanofluid flow along the interior parabolic solar trough collector of an aircraft wing. It is revealed that the energy optimization of the system is upsurged by encouraging nanoparticle volume fraction. The hydrothermal behavior and entropy analysis of buoyancy driven magnetohydrodynamic hybrid nanofluid flow within an octagonal enclosure fitted with fins was investigated by Ref. [21]. Spectral simulation on the flow patterns and thermal control of radiative nanofluid spraying on an inclined revolving disk considering the effect of nanoparticle diameter and solid–liquid interfacial layer was investigated by Ref. [22]. Entropy generation optimization of unsteady radiative hybrid nanofluid flow over a slippery spinning disk was investigated by Ref. [23]. Spectral simulation to investigate the effects of nanoparticle diameter and nanolayer on the ferrofluid flow over a slippery rotating disk in the presence of low oscillating magnetic field was investigated by Ref. [24]. Framing the impacts of highly oscillating magnetic field on the ferrofluid flow over a spinning disk considering nanoparticle diameter and solid–liquid interfacial layer was investigated by Ref. [25]. Spectral quasi linearization simulation of radiative nanofluidic transport over a bended surface considering the effects of multiple convective conditions was investigated by Ref. [26].

The thermal Amelioration in heat transfer rate using Oldroyd-B model hybrid nanofluid by CNTs-based kerosene oil flow in solar collector applications was investigated by Ref. [27]. The result show that SWCNT/kerosene nanofluid has better thermodynamic capability than SWCNT-MWCNT/kerosene nanofluid. Thermal efficacy of SWCNT-MWCNT/Kerosene over SWCNT/kerosene is seen with a minimum of 2.399326 %. The hydrogen energy storage optimization in solar-HVAC using Sutterby nanofluid via Koo-Kleinstreuer and Li (KKL) correlations mode was investigated by Ref. [28]. Thermal characterization of coolant Maxwell type nanofluid flowing in parabolic trough solar collector (PTSC) used inside solar powered ship application was investigated by Ref. [29]. Computational study of heat transfer in solar collectors with different radiative flux models was investigated by Ref. [30]. Thermal examination of chemical interaction and thermophoretic diffusion of Williamson fluid flow across Riga Plate surface with nonlinearity radiation flux was investigated by Ref. [31].

The connection between a liquid and a solid surface is determined by surface texture, chemical characteristics, and temperature, among other variables. The slip condition is a fundamental aspect in this interaction that determines whether the liquid will stick to or slide across the surface [32]. Understanding slip conditions is important, particularly in engineering, biology, and nano technology, where liquid-solid interactions play a significant role. This article explores the significance of slip situations and their applications. Beavers and Joseph [33] first proposed the idea of slip conditions and convective slip conditions. The two primary types of slip conditions include the no-slip condition and the slip condition. Nonetheless, according to the slip condition, when a fluid moves across a solid surface, there are differences in speed between the two at their border. This condition comes in multiple forms, such as the Navier slip condition, Maxwell slip condition, and convective slip condition. The convective slip condition refers to a situation where the velocity of a fluid at its boundary is proportional to the velocity gradient [34]. This means that if there is an increase in the velocity gradient, the slip velocity also increases. This condition is often used for fluids with non-Newtonian properties or those that are highly viscous. Understanding the behavior of fluids near solid surfaces and designing many engineering applications, such as microfluidics, lubrication, and drag reduction, require considering slip conditions. By employing the slip and convective condition. Khan et al. [35] studied the unsteady flow of a hybrid nanofluid on a stretched sheet under the influence of a magnetic field and radiation effects. The authors considered two types of boundary conditions: slip and convective. The slip boundary condition accounts for the horizontal velocity at the surface, while the convective boundary condition takes into account the transfer of heat induced by fluid flow. Both of these conditions are classified as boundary conditions. The energy equation includes the radiative flux to account for radiation effects. The study conducted by Ref. [36] provides insights into the behavior of a hybrid nanofluid under mixed convection conditions and the effect of slip conditions over a shrinking surface. The study conducted by Ref. [37] considers a rotating disk as the surface and investigates the influence of slip effects on the flow behavior. Based on these findings, the authors propose that their work could aid in developing more effective heat transfer systems.

Entropy generation is an important field of thermodynamics that refers to the gradual dissipation of energy within a system. As solar energy becomes increasingly important, scientists are intensifying their efforts to comprehend the impact of entropy generation on this renewable resource. As we work towards a future that relies on solar energy for sustainability, investigating the mechanisms behind entropy generation can lead to new and creative methods for optimizing energy efficiency and reducing waste. Bejan [38] investigated entropy production and developed a method to maximize the efficiency of destroying a system. Bejan's effort offers a helpful tool for scientists and engineers who are particularly interested in examining entropy generation [15,39]. In addition, the entropy of a system is significantly impacted by solar radiation since it serves as the primary energy source for numerous physical and biological activities. In regards to this, Obalalu et al. [40] investigated the entropy production analysis of mechanical energy in solar-powered airplanes by employing the thermal performance of a hybrid nanofluid with the goal of investigating the possibility of sustainable and renewable energy usage. A study was carried out by Ref. [41] to evaluate the thermal transmission performance and entropy generation analysis of solar water pumps. The study took into account the effects of thermal radiation and heat generation, in addition to viscous dissipation.

When nanoparticles are introduced into a non-Newtonian base fluid, the resultant fluid is typically classified as a non-Newtonian nanofluid due to the altered rheological behavior [42]. The utilization of non-Newtonian models is essential for investigating the

thermohydraulic properties of nanofluids with their heat transfer and flow dynamics. So, in this current research study, we are examining the properties of a non-Newtonian Williamson fluid (WF). The WF model can be used to explain the rheological behavior of some complicated fluids, such as polymer solutions and liquids. crystals. J.B. Williamson first introduced this mathematical model [43]. With the aid of an equation model, he created a framework for understanding how pseudo-plastic fluids flow and then demonstrated the validity of the theory using experimental evidence. Researchers used the WF model to depict the properties of numerous complex fluids, including liquid crystal polymers, lyotropic liquid crystals, and some surfactant solutions. This model has also been used to investigate flow dynamics in microfluidic devices and to generate novel materials with customizable rheological characteristics. The WF model may be useful for investigating nanofluids, which are fluids in which nanoparticles are suspended. Nanofluids have drawn interest from scientists and engineers in many sectors, including heat transmission, energy conversion, and biological applications. The rheological behavior of nanofluids can be complicated because of the interaction between the fluid and suspended nanoparticles. The Williamson fluid model offers a way to comprehend this behavior. The viscosity and other rheological characteristics, which are significant in understanding how well they operate in various applications, can be predicted by the nanofluid model [44]. For instance, during heat transfer activities, the viscosity of the nanofluid will influence its capacity to transport heat. Thus, it is crucial to understand their rheological behavior to create more productive systems. In general, the use of the Williamson fluid model can be beneficial in comprehending the characteristics of intricate fluids such as nanofluids, and it may also assist in enhancing the performance of new materials and technologies. Obalalu et al. [45] demonstrated how to utilize knowledge about Williamson fluid (WF) to construct a model for simulating steady hydromagnetic nanofluid flow, while also considering the impact of thermal radiation. The numerical investigation carried out by Ref. [46] examined the non-Newtonian WF flow over a permeable stretching surface in the existence of nonlinear radiative slip motion. Numerous scientists are currently engaged in developing this novel concept of pseudo-plastic fluid [47–51].

Due to the rising demand for effective heat management in industrial and technological processes, researchers focusing on heat transfer analysis are working towards finding a prompt solution to the problem of overheating heating systems. This study aims to evaluate the thermal efficiency of a solar-powered tractor using a nano-metal shaped factor, and a parabolic trough solar collector (PTSC) installed inside the solar-powered tractor.

The study takes into consideration the impact of these elements on the overall thermal performance. The thermal performance of the system was analyzed in this study using two tested working fluids: Cu-engine oil and Ag-engine oil nanofluids. We advocate for the utilization of a cost-effective scaled process to manufacture solar panels for selective nanofluids that can be used in engine oil. The performance of solar thermal conversion demonstrated by the preparations for nanofluids are excellent in terms of their durability. The development of an efficient solar thermal collector for volumetric or bulk absorption of solar radiation using nanofluids has been successful, thanks to effective preparation techniques. Investigating the thermal efficiency of time-dependent magneto-nanofluid flow within a solar-powered tractor application, our study introduces a novel approach by applying a nano-metal shaped factor. The objective is to enhance tractor performance, driven by the motivation to harness cutting-edge nanotechnology for sustainable agricultural practices. By utilizing nano-metal shaped factor, the collector has achieved a steady-state temperature that is around 5 % higher than the temperature reached by conventional nanofluids used in surface absorption solar devices [52]. Also, this study investigates the impact of several factors such as heat generation, thermal radiation, viscous dissipation, porous materials, and thermal dissipation on heat exchange analysis. The nanofluid with the nano-metal shaped factor can be used in the tractor's cooling system. As the tractor operates under the sun, the coolant circulates through the engine and various components to regulate their temperatures. The movement of the Non-Newtonian WF is studied to understand the propagation of entropy, and the Chebyshev collocation spectral Method (CCSM) is utilized as the primary solution strategy for the formulation. Tables and figures are presented to demonstrate the effects of fluid velocity, fluid temperature, drag force, and heat transfer rate. This article provides two important contributions. Firstly, it introduces a theoretical experiment that has not been carried out before. Secondly, it proposes that the PTSC can function as an energy source for economically developing by making use of the light and heat emitted by the sun.

2. Investigation regarding the flow model

The mathematical expressions (1) represent a flatness sheet that moves horizontally and expands non-uniformly [20,53].

$$U_w(x,t) = bx/(1 - \xi t), \tag{1}$$

where b is the initial rate at which expansion occurs. Equation (1) provides the temperature of a surface that is isolated, and at x=0, it is presumed to be constant.

$$T_w(x,t) = T_\infty + b^*x/(1 - \xi t), \tag{2}$$

Where b^* is temperature variation, T_∞ denoted ambient temperature, T_w stand for wall temperature.

$$B(t) = \frac{B_0}{\sqrt{1 - \xi t}}, \tag{3}$$

According to equation (3), a magnetic force of constant intensity $B(t)$ is applied perpendicular to the direction of flow. However, the resulting induced magnetic force is deemed insignificant when compared to the applied B. The standard base fluid for engine oil (EG) was modified by the addition of two nanoparticles: silver (Ag) and copper (Cu). The geometry of the flow model located within the parabolic trough solar collector is depicted as follows in Fig. 2.

2.1. Suppositions and terms of the system

The assumptions provided below have formed the basis for constructing the mathematical formulation.

❖ Thermal radiative flow
❖ Unsteady 2-D laminar flow, Joule heating.
❖ Magnetic field, Heat generation, Nano solid-particles shape-factor.
❖ Non-Newtonian Williamson fluid, Boundary-layer approximations.
❖ Porousness of material, Velocity slip, Single phase (Tiwari-Das) scheme.
❖ The second law of thermodynamics, Flow having viscid dissipation properties,
❖ Silver (Ag) and Copper (Cu), Convective condition, Engine oil (EG) as Base fluid.

2.2. The tensor of stress in non-Newtonian WF

The non-Newtonian WF can be described by the following tensor of stress [54]:

$$S = -pI + \tau_{ij}, \tag{4}$$

Where τ_{ij} is the additional stress-tensor

$$\tau_{ij} = (\mu_\infty + (\mu_0 - \mu_\infty) / (1 - \beta c))Z_1, \tag{5}$$

Then c is defined as the first Rivlin Eriksen tensor, where $c = \sqrt{\frac{\pi}{2}}$; where $\pi = trace(z_1^2)$, μ_0 is restrictive viscidness at zero shearing rates. When $\beta > 0$ is defined as steady time. Also, μ_∞ restrictive viscosities at infinite.

In addition, in this case, we assumed that $\beta > 0$ and $\mu_\infty = 0$. Therefore, equation (3) can be expressed as:

$$\tau_{ij} = ((\mu_0) / (1 - \beta c))Z_1, \tag{6}$$

Which may be expressed using the binomial expansion in the following manner:

$$\tau_{ij} = (\mu_0(1 + \beta c))Z_1, \tag{7}$$

2.3. Model equations

Considering the aforementioned assumptions, the equations that control the motion of the viscous non-Newtonian WF model are as follows [55]:

$$\frac{\partial R_1}{\partial x} + \frac{\partial R_2}{\partial y} = 0, \tag{8}$$

$$\frac{\partial R_1}{\partial t} + R_1 \frac{\partial R_1}{\partial x} + R_2 \frac{\partial R_2}{\partial y} = \frac{\mu_{nf}}{\rho_{nf}} \frac{\partial^2 R_2}{\partial y^2} - \frac{\sigma_{nf}}{\rho_{nf}} B^2(t)R_1 - \frac{\mu_{nf}}{\rho_{nf}} \left[\left(\frac{\partial R_1}{\partial y}\right)\left(\frac{\partial^2 R_1}{\partial y^2}\right) \right] \sqrt{2}\beta - \frac{\mu_{nf}}{\rho_{nf}k}R_1, \tag{9}$$
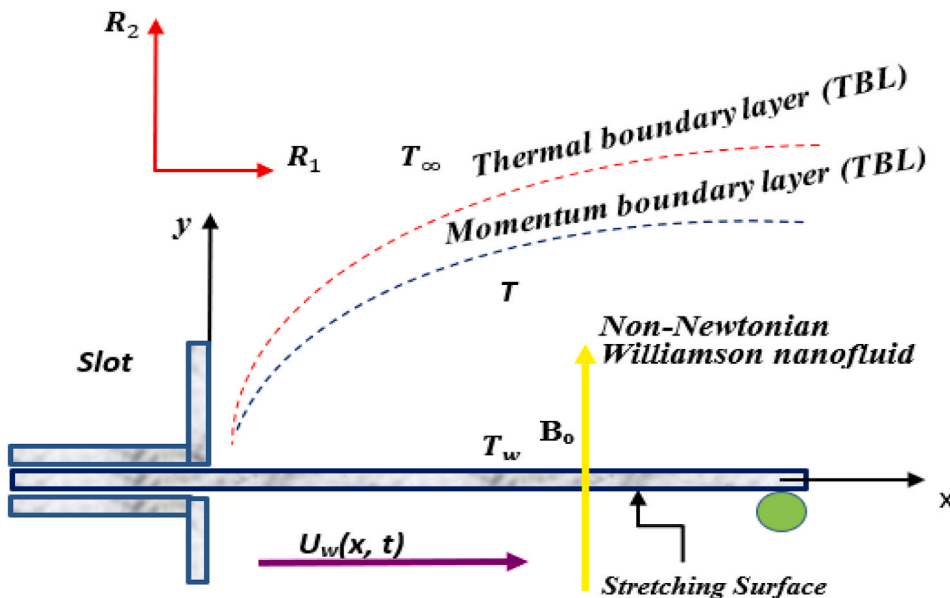

Fig. 2. Geometrical diagram of the flow model.

$$\frac{\partial T}{\partial t} + R_1 \frac{\partial T}{\partial x} + R_2 \frac{\partial T}{\partial y} = \frac{1}{(\rho C_p)_{nf}} \left[k_{hnf} \left(\frac{\partial^2 T}{\partial y^2} \right) - \left(\frac{\partial q_r}{\partial y} \right) + Q(T - T_\infty) \right] + \frac{\sigma_{nf}}{(\rho C_p)_{nf}} B^2(t) R_1^2 + \frac{\mu_{nf}}{(\rho C_p)_{nf}} \left(\frac{\partial R_1}{\partial y} \right)^2 \tag{10}$$

Subjected to:

$$R_1(x,0) = U_w + N_x \left(\frac{\partial R_1}{\partial y} \right), \quad -k_0 \left(\frac{\partial T}{\partial y} \right) = h_f(T_w - T), R_2(x,0) = R_w, R_1 \longrightarrow 0, T \longrightarrow T_\infty, \text{ as } y \longrightarrow \infty.. \tag{11}$$

In the above equations, the velocity of the moving fluid is made up of the following components: $\overleftarrow{R} = [R_1(x,y), R_2(x,y), 0]$. where the respective terms μ_{nf} dynamic viscosity, T_∞ ambient temperature, ρ_{nf} density k_0 thermal conductivity of solid, σ_{nf} electric conductivity, R_w the porosity of the encompassing plate, k_{hnf} thermal conductance, h_f heat transfer coefficient, $(\rho C_p)_{nf}$ specific heat, N_x slip length, t time. In addition, it is important to take into account the physical features, such as the surface that was traditionally heated and lost its heat through conduction (also called Newtonian heating), as well as how the shear stress created on a surface directly affects the speed of the fluid near the surface (the slip condition).

2.4. Thermophysical characteristics of non-Newtonian Williamson-nanofluid

The thermophysical properties of the nanofluid were calculated using the nanoparticles and the EO base fluid.

$$\mu_{nf} = \frac{\mu_f}{(1-\varphi)^{2.5}}, \sigma_{nf} = \sigma_f \left(1 + \frac{3\left(\frac{\sigma_s}{\sigma_f} - 1 \right)\varphi}{2 + \frac{\sigma_s}{\sigma_f} - \left(\frac{\sigma_s}{\sigma_f} - 1 \right)\varphi} \right), \rho_{nf} = (1-\varphi)\rho_f + \varphi\rho_s \ (\rho C p)_{nf} = (\rho C p)_f(1-\varphi) + (\rho C p)_s,$$

$$\frac{k_{hnf}}{k_{gf}} = \frac{(k_s + (m-1)k_f) - (m-1)\varphi(k_f - k_s)}{(k_s + (m-1)k_f) + \varphi(k_f - k_s)} \tag{12}$$

The importance of nano molecules is identified by their specific shapes and how those shapes influence their impact. Fig. 3 presents the functional component evaluations for various element shapes. Nanomolecules in particle shape consist of spheres, hexahedrons, tetrahedrons, columns, and lamina [56]. However, a hexahedron is a type of polyhedron that has six sides, and each side is shaped like a square. Nanomolecules that are approximately spherical and have a diameter of fewer than 100 nm are referred to as sphere-shaped nano molecules. Tiny objects, also known as nanoparticles, can be created from a wide range of substances, such as metals, polymers, and ceramics. The tetrahedron is a type of geometric form that is characterized by having four faces that are in the shape of triangles and four vertices. The specific shape that a nano molecule takes influences its physicochemical features, including its surface area, reactivity, and capacity to interact with other molecules. Due to their versatility in shape and size, nano molecules have the potential to be beneficial for a wide range of applications, including drug delivery, energy storage, and the construction of electronic devices.

2.5. Nanoparticles characteristics and Basefluid

Table 1 lists the important properties of the EG utilized as Base Fluid and the various NP types employed in the current study.

Many engineering applications are based on heat exchangers to transfer heat between two or more fluids. Some applications include solar drying of agricultural products, tube-in-tube heat exchangers, refrigeration, solar water heating, automobile radiators, power plants, oil refineries, and solar collectors [53]. Heat exchangers are essential to the operation of any system and must function properly. To enhance the efficiency of a solar thermal system, a strategy is to use a heat exchanger to redirect the hot fluid to another system. However, the effectiveness of these technologies is often limited by the thermal conductivity of the transfer fluid, even though there are multiple methods available to improve their efficiency. However, engine oil (EO), consisting of intricate blends of base oils and additives that offer a variety of physical and chemical qualities, including viscosity, lubricity, wear prevention, and oxidation resistance, has attracted great attention. Even though industrialization has spread widely, advances in copper-based engine oil are eagerly anticipated. The smooth and effective operation of an engine is dependent on a variety of beneficial characteristics of engine oil. By providing lubrication, cooling, cleaning, corrosion prevention, sealing, and viscosity management, engine oil contributes significantly to the lifetime and efficiency of an engine. Lubricating the engine's moving parts with engine oil prevents them from rubbing against one another during operation, which in turn reduces wear and friction and shields the engine from rust and oxidation.

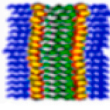| Types of nanoparticles	Sphere	Hexahedron	Tetrahedron	Column	Lamina
Shape m					
	$m = 3$	$m = 3.7221$	$m = 4.0613$	$m = 6.3698$	$m = 16.1576$

Fig. 3. The practical shaped element standards for various particle shapes [56].

Table 1

Thermo-physical characteristics for the base fluid and hybrid nanofluid [57].

Physical property	EO	Cu	Ag
$\rho/\ (kg.m^{-3})$	884	8933	10500
$k/\ (W.mK)$	0.144	401.0	429
$C_p/\ (J.kgK)$	1910	385.0	235
$\sigma\ (S\ m^{-1})$	0.125×10^{-11}	5.96×10^{7}	6.3×10^{7}

Copper is known for its excellent electrical conductivity, making it a preferred choice for electrical wiring and components. Silver has even higher electrical conductivity. Both Silver and Copper have high thermal conductivity, making them suitable for applications involving heat transfer, such as in heat exchangers and cooling systems.

2.6. Rosseland approximation (RA)

The RA is a mathematical technique commonly used in astrophysics and radiative heat transfer to estimate the average opacity of a dense material that is impenetrable to radiation. The non-Newtonian Williamson-radiative flow only covers a small amount of space, which results in the thickening of nanofluid. Since the energy formula is both highly nonlinear in temperature (T) and hard to comprehend numerically, a significant amount of simplification may be accomplished when the thermal gradients within the stream are minimal. In these situations, the RA formula can be linearized into temperature (T_∞) by substituting (T^3) with the (T_∞)^3. Equation (10) employs RA calculation for radiative flux, which is represented as [29]:

$$qr = -\frac{4\sigma^*}{3k^*}\frac{\partial T}{\partial y}, \tag{13}$$

σ^* described as Stefan Boltzmann and k^* signifies the absorption coefficient.

3. Problem solution

The mathematical partial derivative model is transformed into an invariant ordinary derivative via the following similarity variable as provided by [41].

$$\eta(x,y) = \sqrt{\frac{b}{v_f(1-\xi t)}}y, \theta(\eta) = \frac{T-T_\infty}{T-T_\infty}, \tag{14}$$

and

$$\psi(x,y) = \sqrt{\frac{v_f b}{(1-\xi t)}}xf(\eta)$$

And

$$R_1 = \frac{\partial\psi}{\partial y}, \text{and } R_2 = -\frac{\partial\psi}{\partial x}, \tag{15}$$

Employing the transformation variables of equation (14) - (15) into (8) - (10), a dimensionless invariant model is obtained as:

$$\zeta(f''f'') + f'' + \lambda_a\lambda_b(ff'' - f'^2) - A f' - K_N f' - \lambda_a\lambda_b M f' - A \frac{\eta}{2}f'' = 0 \tag{16}$$

$$\theta''\left(1 + \frac{1}{\lambda_d}R_N\ Pr\right) + Pr\ M\ \delta_c f'^2\frac{\lambda_a}{\lambda_b} + \frac{Pr\ \delta_c}{\lambda_a\lambda_b}f'^2 + \frac{Pr\ Q}{\lambda_c}f'^2 + \frac{Pr\ \lambda_c}{\lambda_e}\left[f\theta' - A\left(\theta + \frac{\eta}{2}\theta'\right)\right] \tag{17}$$

Subjected to

$$f'(0) = 1 + \chi f''(0), f(0) = S, f'(\gamma)\longrightarrow 0, \theta'(0) = -B_i(1-\theta(0)), \theta(\gamma)\longrightarrow 0, \text{as}\quad \gamma\longrightarrow\infty, \tag{18}$$

Here, a ≤ I ≤ b (17) and (18) represent the physical thermal characteristics that are relevant to W–NF.

$$
\begin{cases}
\lambda_a = (1-\varphi)^{2.5}, \\[2mm]
\lambda_b = \left(1 - \varphi + \varphi\left(\dfrac{\rho_s}{\rho_f}\right)\right), \\[2mm]
\lambda_c = \left((1-\varphi) + \varphi\dfrac{(\rho C_p)_s}{(\rho C_p)_f}\right), \\[2mm]
\lambda_d = \left(1 + \dfrac{3\left(\dfrac{\sigma_s}{\sigma_f} - 1\right)\varphi}{\left(2 + \dfrac{\sigma_s}{\sigma_f}\right) - \left(\dfrac{\sigma_s}{\sigma_f} - 1\right)\varphi}\right), \\[4mm]
\lambda_e = \dfrac{(k_s + (m-1)k_f) - (m-1)\varphi(k_f - k_s)}{(k_s + (m-1)k_f) + \varphi(k_f - k_s)}.
\end{cases}
\tag{19}
$$

Table 2 lists the thermophysical characteristics of nanofluids as well as the symbols that were employed in this research. The drag coefficient (Cf) at a moving flatness horizontal sheet is defined as:

$$
C_f = \frac{\tau_w}{\rho_{nf} U_w^2},
\tag{20}
$$

In consideration of equation (9), the following dimensionless transformations are applied to obtain:

$$
C_f Re_x^{1/2} = \frac{f''(0)}{\lambda_a}\left[1 + \frac{\zeta}{2}(f''(0))^2\right],
\tag{21}
$$

The heat transfer rate (Nu_x) at a moving flatness horizontal sheet is defined as:

$$
Nu_x = \frac{x q_w}{k_f(T_w - T_\infty)},
\tag{22}
$$

In consideration of equation (10), the following dimensionless transformations are applied to obtain:

Table 2
below lists the governing equation's control parameters.

Parameters	Formula	Symbols Value
WF parameter	$\zeta = \beta x \sqrt{\dfrac{2b^3}{v_f(1-\xi t)^3}}$	ζ
Biot number	$B_i = \dfrac{h_f}{k_0}\sqrt{\dfrac{v_f(1-\xi t)}{b}}$	B_i
Heat generation	$Q = \dfrac{Q_0}{(\rho C_p)_f b}$	Q
Eckert number	$Ec = \dfrac{U_w^2}{(C_p)_f(T_w - T_\infty)}$	Ec
Solar radiation	$R_N = \dfrac{16}{3}\dfrac{\sigma^* T_\infty^3}{k^* v_f(\rho C_p)_f}$	R_N
slippery factor	$\chi = \sqrt{\dfrac{b}{v_f(1-\xi t)}} N_x$	χ
Suction/Injection Parameter	$S = -U_w\sqrt{\dfrac{(1-\xi t)}{v_f b}}$	S
Porous medium	$K_N = \dfrac{v_f}{bk}$	K_N
Prandtl number	$Pr = \dfrac{v_f}{\alpha_f}$	Pr
Porous medium	$K_N = \dfrac{v_f(1-\xi t)}{bk}$	K_N
Entropy generation	$N_G = \dfrac{E_G b^2 T_\infty^2}{k_f(T_w - T_\infty)^2}$	N_G
Thermal diffusivity	$\alpha_f = \dfrac{k_f}{(\rho C_p)_{hnf}}$	α_f
Magnetic field	$M = \dfrac{\sigma_f B_0^2}{b\rho_f}$	M

$$Re_x^{1/2} Nu_x = -\frac{k_{nf}}{k_f}[(1 - Nr)\acute{\theta}(0)] \tag{23}$$

Where τ_w, and q_m are:

$$\tau_w = \mu_{nf}\left(\frac{\partial R_1}{\partial y} + \frac{\xi}{\sqrt{2}}\left(\frac{\partial v_1}{\partial y}\right)^2\right)_{y=0} \tag{24}$$

and

$$q_w = -k_{nf}\left(\left(1 + \frac{16}{3}\frac{\sigma^* T_\infty^3}{k^* v_f (\rho C_p)_f}\right)\left(\frac{\partial T}{\partial y}\right)\right)_{y=0}$$

4. Entropy generation analysis (EG)

The production of entropy is an effective instrument that can be employed to evaluate the effectiveness of fluid flow processes, including heat transmission and fluid mixing. When entropy production increases, productivity tends to decrease, and more energy is lost. Engineers can construct fluid flow systems with minimal entropy formation and maximum efficiency if they have a clear understanding of the elements that lead to their creation. This has the potential to drastically cut down on energy use and subsequent environmental damage. There is a connection between solar energy and the production of entropy. Solar power is a form of renewable energy generated by the sun's radiation, and it can be converted into various forms of useable energy like electricity or heat. The EG is described as [58]:

$$E_G = \frac{k_{nf}}{T_\infty^2}\left[\left(\frac{\partial T}{\partial y}\right)^2 + \frac{16}{3}\frac{\sigma^* T_\infty^3}{k^* v_f (\rho C_p)_f}\left(\frac{\partial T}{\partial y}\right)^2\right] + \frac{\sigma_{nf} B^2(t) R_1^2}{T_\infty} + \frac{\mu_{nf} R_1^2}{kT_\infty} + \frac{\mu_{nf}}{T_\infty}\left(\frac{\partial R_1}{\partial y}\right)^2 \tag{25}$$

The first signifies the loss of heat transfer efficiency, while the second parameter represents the increase in entropy caused by viscosity. The third and fourth parameters are associated with the penetrable medium and magnetic field, and viscous dissipation, respectively. the dimensionless entropy generation can be described by the value of N_G:

$$N_G = \frac{E_G \mu_f T_w^2}{k_f (T_w - T_\infty)^2} \tag{26}$$

Established on equations (14) and (15), the dimensionless equation of entropy production can be achieved next.

$$N_G = Re\left[\varphi_d(1 - Nr)\theta'^2 + \frac{1}{\lambda_a}\frac{Br}{\Omega}\left(f''^2 + K_N f'^2 + \lambda_a \lambda_d M f'^2\right)\right], \tag{27}$$

Here, Ω indicates the dimensionless temperature, Re is the Reynolds number, Br is the Brinkman number.

5. Chebyshev Collocation Spectral Method (CCSM)

5.1. An expression for finding the derivative of a Chebyshev polynomials expansion

A useful numerical tool for solving differential equations over a domain is the CCSM. To obtain an approximation for the solution of the differential equation, this particular type of spectral approach uses Chebyshev polynomials as its basis functions. The Chebyshev polynomials $\mathscr{H}_m(Q)$ of degree m can be written in an analytic form as follows:

$$\mathscr{H}_m(Q) = m\sum_{j=0}^{\left[\frac{m}{2}\right]}(-1)^j 2^{m-2j-1}\frac{(m-j-1)}{(j)!(n-2j)!}Q^{m-2j}, \tag{28}$$

Here, $\left[\frac{m}{2}\right]$ represents the integer portion of $\frac{m}{2}$. By implementing a change in the variables $Q = 2y - 1$, we characterize a class of polynomials known as shifted Chebyshev polynomials (SCP). The SCP is shown as

$$B\mathscr{H}_m(y) = \mathscr{H}_m(2y - 1) = \mathscr{H}_{2m}(\sqrt{y}), \tag{29}$$

This expression is general, therefore we can apply it to the interval $[0, \eta_\infty]$.

$$f(y) = \sum_{j=0}^{\infty} a_i B\mathscr{H}_j(y), \tag{30}$$

the coefficients a_i are determined as

$$a_0 = \frac{1}{\pi} \int_0^1 \frac{f(x)B\mathscr{H}_0(y)}{\sqrt{x - x^2}} dx \tag{31}$$

And

$$a_i = \frac{2}{\pi} \int_0^1 \frac{f(x)B\mathscr{H}_j(y)}{\sqrt{x - x^2}} dx \tag{32}$$

Where j = 1, 2 …. In practical implementation, the first (n + 1) elements of SCP are taken into account. We obtain

$$f_n(y) = \sum_{j=0}^n a_i B\mathscr{H}_j(y), \tag{33}$$

The following expression gives the analytic formulation of the SCP $B\mathscr{H}_m(y)$ of degree m:

$$B\mathscr{H}_m(y) = m \sum_{i=0}^m (-1)^{m-v} \frac{2^{2i}(m + v - 1)!}{(2v)!(m - v)!} y^v, \tag{34}$$

Where $m = 1, 2 \ldots$ in addition, the basic approximation expression for the derivative of $f_n(y)$ can be found in the theorem that is presented below.

5.2. Theorem

Let r be an integer number, and $f(y)$ is the approximated value via SCP as equation (33), then.

$$\beta^{(p)}(f_n(y)) = \sum_{j=p}^n \sum_{v=0}^j a_i \sigma_{j,v,p} y^{v-p}, \tag{35}$$

Where $\sigma_{j,v,p}$ is assumed as

$$B\mathscr{H}_m(y) = (-1)^{j-v} \frac{2^{2v} j(j + v - 1)! v!}{(j - v)!(2k)!(m - v)!}, \tag{36}$$

Proof: This theorem can be proved directly by employing equation (34) and certain properties of the SCP procedure solution.

5.3. Application of CCSM

Now, we apply this approach to numerically solve the system of ODE in equation (16) and (17)

$$f_n(\eta) = \sum_{j=0}^n a_i B\mathscr{H}_j(\eta), \tag{37}$$

And

$$\theta_n(\eta) = \sum_{j=0}^n b_i B\mathscr{H}_j(\eta), \tag{38}$$

via applying equations (16)–(18) as well as theorem 1, we get

$$\zeta \left(\sum_{j=1}^n \sum_{v=1}^j a_i \sigma_{j,v,1} \eta^{v-1} \right) \left(\sum_{j=2}^n \sum_{v=2}^j a_i \sigma_{j,v,2} \eta^{v-2} \right) + \sum_{j=3}^n \sum_{v=3}^j a_i \sigma_{j,v,3} \eta^{v-3} + \lambda_a \lambda_b \left(\left(\sum_{j=0}^n a_i B\mathscr{H}_j(\eta) \right) \left(\sum_{j=2}^n \right.\right.$$
$$\times \left. \sum_{v=2}^j a_i \sigma_{j,v,2} \eta^{v-2} \right) - \left(\sum_{j=1}^n \sum_{v=1}^j a_i \sigma_{j,v,1} \eta^{v-1} \right)^2 \right) - A \left(\sum_{j=1}^n \sum_{v=1}^j a_i \sigma_{j,v,1} \eta^{v-1} \right) - K_N \left(\sum_{j=1}^n \sum_{v=1}^j a_i \sigma_{j,v,1} \eta^{v-1} \right) - \lambda_a \lambda_b M \left(\sum_{j=1}^n \right.$$
$$\times \left. \sum_{v=1}^j a_i \sigma_{j,v,1} \eta^{v-1} \right) - A \frac{\eta}{2} \left(\sum_{j=2}^n \sum_{v=2}^j a_i \sigma_{j,v,2} \eta^{v-2} \right) = 0, \tag{39}$$

$$\left(\sum_{j=2}^n \sum_{v=2}^j b_i \sigma_{j,v,2} \eta^{v-2} \right) \left(1 + \frac{1}{\lambda_d} R_N \, Pr \right) + \frac{\lambda_a}{\lambda_b} \, Pr \, M\delta_c \left(\sum_{j=1}^n \sum_{v=1}^j a_i \sigma_{j,v,1} \eta^{v-1} \right)^2 + \frac{Pr \, \delta_c}{\lambda_a \lambda_b} \left(\sum_{j=2}^n \sum_{v=2}^j a_i \sigma_{j,v,2} \eta^{v-2} \right)^2 + \frac{Pr \, Q}{\lambda_c} \sum_{j=0}^n b_i B\mathscr{H}_j(\eta)$$
$$+ \frac{Pr \, \lambda_c}{\lambda_e} \left[\sum_{j=0}^n a_i B\mathscr{H}_j(\eta) \left(\sum_{j=1}^n \sum_{v=1}^j b_i \sigma_{j,v,1} \eta^{v-1} \right) - A \left(\sum_{j=0}^n a_i B\mathscr{H}_j(\eta) + \frac{\eta}{2} \left(\sum_{j=1}^n \sum_{v=1}^j b_i \sigma_{j,v,1} \eta^{v-1} \right) \right) \right] \tag{40}$$

Furthermore, we combine equations (39) and (40) at (m–n+1) points

$$\zeta \left(\sum_{j=1}^{n} \sum_{v=1}^{j} a_i \sigma_{j,v,1} \eta_{\mathscr{H}}^{v-1} \right) \left(\sum_{j=2}^{n} \sum_{v=2}^{j} a_i \sigma_{j,v,2} \eta_{\mathscr{H}}^{v-2} \right) + \sum_{j=3}^{n} \sum_{v=3}^{j} a_i \sigma_{j,v,3} \eta_{\mathscr{H}}^{v-3} + \lambda_a \lambda_b \left(\left(\sum_{j=0}^{n} a_i B \mathscr{H}_j(\eta) \right) \left(\sum_{j=2}^{n} \right. \right.$$

$$\times \sum_{v=2}^{j} a_i \sigma_{j,v,2} \eta_{\mathscr{H}}^{v-2} \right) - \left(\sum_{j=1}^{n} \sum_{v=1}^{j} a_i \sigma_{j,v,1} \eta_{\mathscr{H}}^{v-1} \right)^2 \right) - A \left(\sum_{j=1}^{n} \sum_{v=1}^{j} a_i \sigma_{j,v,1} \eta_{\mathscr{H}}^{v-1} \right) - K_N \left(\sum_{j=1}^{n} \sum_{v=1}^{j} a_i \sigma_{j,v,1} \eta_{\mathscr{H}}^{v-1} \right) - \lambda_a \lambda_b M \left(\sum_{j=1}^{n} \right.$$

$$\times \sum_{v=1}^{j} a_i \sigma_{j,v,1} \eta^{v-1} \right) - A \frac{\eta}{2} \left(\sum_{j=2}^{n} \sum_{v=2}^{j} a_i \sigma_{j,v,2} \eta_{\mathscr{H}}^{v-2} \right) = 0, \tag{41}$$

$$\left(\sum_{j=2}^{n} \sum_{v=2}^{j} b_i \sigma_{j,v,2} \eta_{\mathscr{H}}^{v-2} \right) \left(1 + \frac{1}{R_N} Pr \right) + \frac{\lambda_a}{\lambda_d} Pr M \delta_c \left(\sum_{j=1}^{n} \sum_{v=1}^{j} a_i \sigma_{j,v,1} \eta_{\mathscr{H}}^{v-1} \right)^2 + \frac{Pr \, \delta_c}{\lambda_a \lambda_b} \left(\sum_{j=2}^{n} \sum_{v=2}^{j} a_i \sigma_{j,v,2} \eta_{\mathscr{H}}^{v-2} \right)^2 + \frac{Pr \, Q}{\lambda_c} \sum_{j=0}^{n} b_i B \mathscr{H}_j(\eta)$$

$$+ \frac{Pr \, \lambda_c}{\lambda_e} \left[\sum_{j=0}^{n} a_i B \mathscr{H}_j(\eta) \left(\sum_{j=1}^{n} \sum_{v=1}^{j} b_i \sigma_{j,v,1} \eta_{\mathscr{H}}^{v-1} \right) - A \left(\sum_{j=0}^{n} a_i B \mathscr{H}_j(\eta) + \frac{\eta}{2} \left(\sum_{j=1}^{n} \sum_{v=1}^{j} b_i \sigma_{j,v,1} \eta_{\mathscr{H}}^{v-1} \right) \right) \right] \tag{42}$$

with

$$\sum_{j=0}^{n} (-1)^j a_j = S, \sum_{j=0}^{n} \tau 1_j a_j - \lambda \left(\sum_{j=0}^{n} \tau 2_j a_j \right) = 1, \sum_{j=0}^{n} \tau 1_j b_j - \sum_{j=0}^{n} (-1)^j b_j = B_i \tag{43}$$

The shifted Chebyshev polynomial are utilized to determine appropriate collocation points. The MATHEMATICA software was utilized to calculate unknowns a_j, b_j. $j = 0, 1, ..., n$.

6. Results and discussion

In this section, the effect of controlling parameters on velocity $f'(\eta)$, and temperature $\theta(\eta)$, and entropy generation N_G, drag co-efficient (Cf), and heat transfer rate (Nu_x) for (Cu-Engine oil) and (Ag – Engine oil) nanofluid are presented graphically. The ranges of influencing parameters are: Williamson fluid (WF) parameter ($\zeta = 0.1, 0.2, 0.3$), permeability parameter ($K_N = 1, 2, 3$), thermal radiation (R_N), Eckert number (Ec$= 0.1, 0.2, 0.3$), and heat generation (Q = 1, 2, 3), velocity slip ($\chi = 0.1, 0.2, 0.3$) Reynolds number ($R_e = 1, 5, 7$), volume friction of nanoparticles (φ), and Brinkman number ($B_r 0.1, 0.15, 0.2$), Biot number ($B_i 0.1, 0.5, 1.0$), volume friction of nanoparticles ($\varphi = 0.01, 0.15, 0.2$).

6.1. Impact of Williamson fluid (WF) parameter (ζ) on velocity $f'(\eta)$, and temperature $\theta(\eta)$ for (Cu-Engine oil) and (Ag – Engine oil) nanofluid

The physical performance of velocity and thermal distribution for the WF parameter is displayed graphically in Fig. 4(a and b). Non-Newtonian fluids are defined as fluids that do not obey Newton's law of viscosity [59]. This law stipulates that the rate of deformation (shear rate) of a fluid should be proportionate to the amount of shear stress that is applied to the fluid. To put it another way, the viscosity of a Newtonian fluid remains the same regardless of the shear rate that is applied to it. However, Williamson fluid is a particular kind of non-Newtonian fluid that is distinguished by its shear-thinning properties. In Fig. 4a, it has been shown that the velocity of non-Newtonian-WF decreases as it approaches the walls. The enhancement of Ag – $Engine$ oil is larger than nanofluid of Cu-Engine oil. Physically, the shear-thinning phenomenon is shown by WF, which simply implies that the viscosity of these fluids reduces as the shear rate increases. In contrast to a Newtonian fluid, the boundary layer's thickness decreases because of the layer with high viscosity located near the surface. Conversely, the temperature profile is noticeably impacted by the WF parameter. However, the
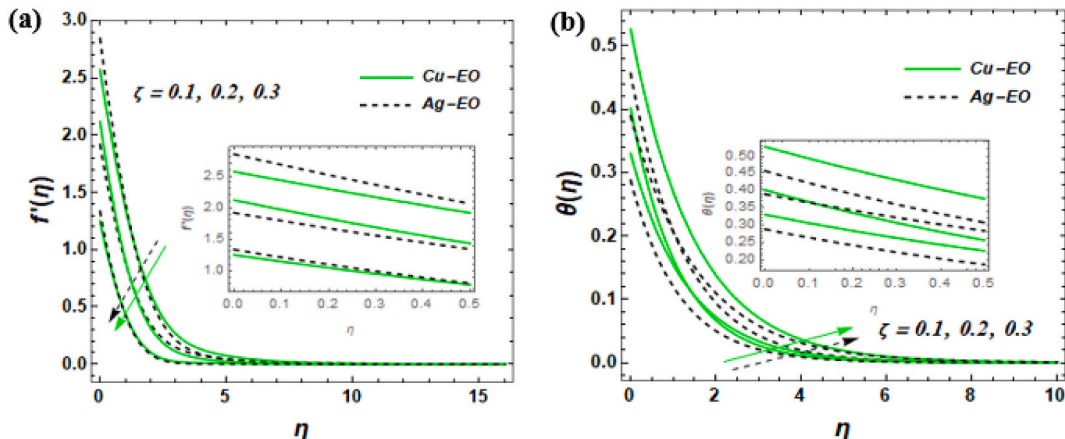

Fig. 4. Imapct of ζ on $f(\eta)$, and $\theta(\eta)$.

WF improves heat transmission due to its non-Newtonian nature. It was observed that the enhancement of *Cu- Engine oil* is greater than the *Ag − Engine oil* nanofluid. As the shear rate is raised, the viscosity of the fluid will drop, which will result in more turbulence and mixing. Because of this, the temperature distribution can get more uniform, and the heat transfer rates increase.

6.2. Influence of permeability parameter (K_N) on velocity $f^{'}(\eta)$, temperature $\theta(\eta)$, and entropy generation N_G for (Cu-Engine oil) and (Ag − Engine oil) nanofluid

The permeability (K_N) in nanofluid flow show how smoothly a fluid can enter a porous material. Furthermore, the fluid velocity for Cu-Engine oil is lower than the Ag- Engine oil. However, as a liquid passes through a porous media, its velocity varies, as described via the velocity field. When the porosity increases, the liquid can flow faster and more freely through the porous media, and the flow rate has the potential to become more uniform. As a result, the fluid's motion is more uniformly distributed across the medium. On the other hand, the fluid velocity is likely to become more heterogeneous whenever the porosity value is low since the liquid has a difficult time passing through the porous media. This implies that the fluid can move more diversely in the velocity distribution (see Fig. 5a). The effect of K_N increases the temperature profile (see Fig. 5b). it was shown that the fluid temperature for Cu-Engine oil is higher than the Ag- Engine oil nanofluid. Physically, the permeability characteristic has a large effect on engine oil's effectiveness. Therefore, the purpose of engine oil is to prevent corrosion and oxidation while also minimizing wear and friction on the engine's moving parts of the solar-powered tractor. The efficiency of an engine can be influenced in several ways via the permeability, which determines how easily oil can flow through the solar-powered tractor engine. An increased permeability characteristic will allow the engine oil to flow more freely throughout the engine, making it possible for it to approach each of the locations requiring lubrication [60]. Fig. 5a shows the impact of K_N on entropy production. The knowledge of entropy creation is important to thermodynamics because it serves to quantify the degree to which a process cannot be reversed [58]. In the context of porous media, the development of entropy is connected to the reduction in availability that occurs as a result of the movement of fluids through the pores' medium. However, the entropy generation for Cu-Engine oil is greater than the Cu-Engine oil nanofluid.

6.3. Influence of velocity slip (χ) on velocity $f^{'}(\eta)$, temperature $\theta(\eta)$, entropy generation N_G for (Cu-Engine oil) and (Ag − Engine oil) nanofluid

Velocity slip is a phenomenon occurring at the boundary between a fluid and a solid surface [61]. The slip boundary condition arises when the velocity of the fluid close to the solid surface is lower than that of the solid surface itself. This may also be stated as the slip velocity. This slip velocity has the potential to have a major impact on the entire performance of the boundary layer (BL), including the layer's thickness and the rate at which it is growing. When the shear force at the BL is high, the BL thickness decreases. As a result, the fluid in the BL must travel a shorter distance before achieving free stream velocity. However, the flow of the BL may well be lowered as a result. velocity slip has the effect of lowering the BL flow by lowering the shear stress at the boundary, which in turn lowers the boundary layer thickness. This behavior is displayed in Fig. 6a. The nanofluid Cu-EO and Ag-EO showed in Fig. 6a illustrate
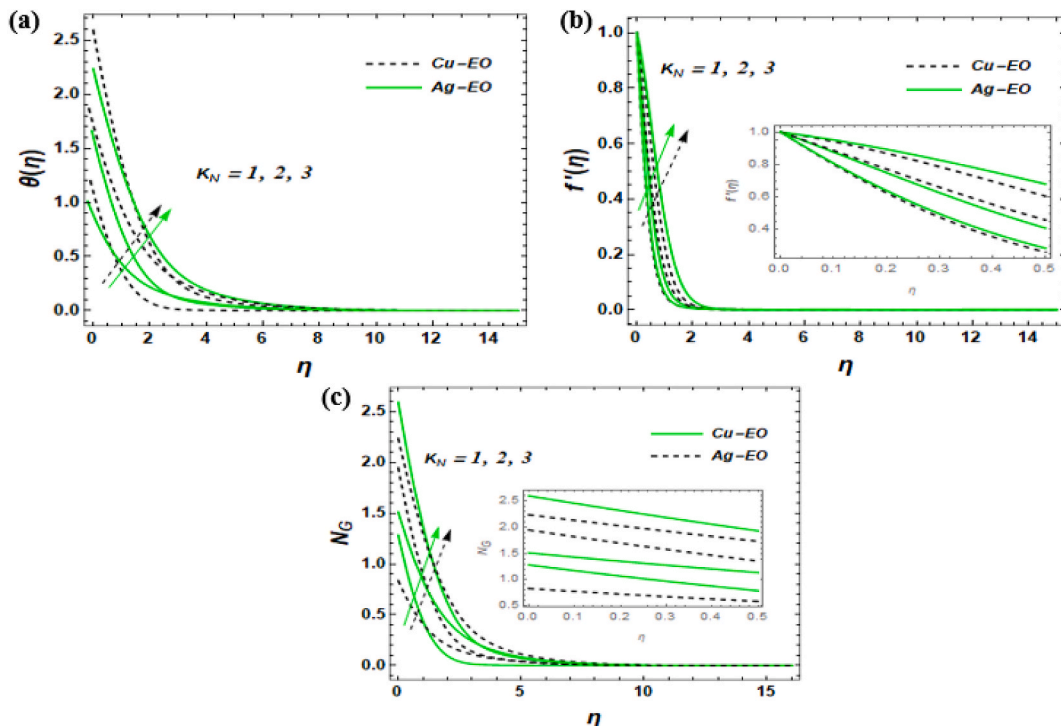

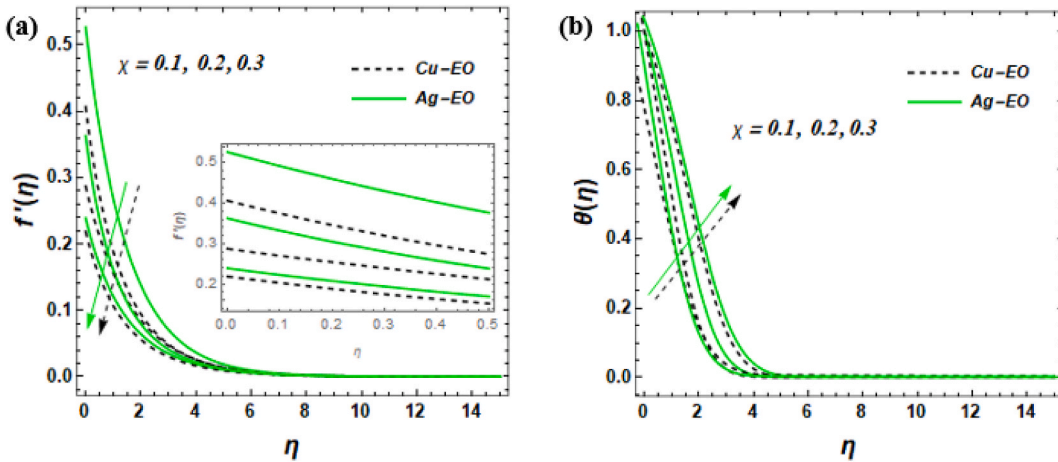**Fig. 5.** Effect of K_N on $f^{'}(\eta)$, $\theta(\eta)$, and N_G.

Fig. 6. Impact of χ on $f(\eta)$, and $\theta(\eta)$.

the impact of χ on fluid temperature. It shows that the nanofluid with the combination Ag-EO has a higher thermal performance than the Cu-EO nanofluid. In addition to improving the efficiency of heat transmission, the velocity slip parameter boosts the Ag-EO nanofluid inside the boundary layer. By increasing fluid mixing, velocity slip improves the flow in a thermal boundary layer.

6.4. Impact of Thermal radiation (R_N), on thermal $\theta(\eta)$, and entropy generation (N_G) for (Cu-Engine oil) and (Ag − Engine oil) nanofluid

Thermal radiation occurs when a material emits electromagnetic waves as a result of its temperature. When a material is heated, it absorbs energy, which is then emitted as electromagnetic waves [61]. This type of radiation is referred to as thermal radiation and is an inherent property of thermal energy. The velocity distribution remains unaffected by the radiation parameter (R_N). However, the occurrence of thermal radiation introduces more heat into the system, leading to an increase in the NF. The temperature field is strengthened as a result of rising values of the thermal radiative term $R_N = (\frac{16}{3} \frac{\sigma^* T_\infty^3}{k^* v_f (\rho C_p)_f})$, which in turn causes an increase in temperature profile. Fig. 7a depicts this kind of performance. Physically, a higher solar radiation parameter shows that Solar radiation is more effective than convection. In addition to this, Solar-powered tractors utilize photovoltaic panels to transform sunlight into electricity, which can be applied to energize the tractor's electric engine or recharge its batteries [16]. The efficiency and performance of solar-powered tractors may be influenced by the favorable effects of thermal radiation. Tractors powered by solar energy are engineered to collect sunlight and convert it into electrical energy, which is a kind of thermal radiation. Because of this, the amount of power that the PV panels create will increase in proportion to the amount of solar radiation that is present. In addition, if the tractor is fitted with a solar concentrator, which directs the sun's rays toward the photovoltaic panel, it is possible to raise the amount of radiation that is emitted and therefore the amount of electricity produced. The physical behavior of Solar radiation parameters (R_N) is exhibited graphically in Fig. 7a it was observed that the production of entropy produce for $Ag − Engine oil$ is higer then Cu-EO nanofluid. Entropy production is significantly influenced by solar radiation, particularly in power production that is reliant on sunlight energy for their operation. Solar radiation can contribute to irreversibility in a thermodynamic process, and the production of entropy is a metric that quantifies the level of irreversibility. solar radiation is expected to boost the production of entropy by inducing irreversible changes in processes related to the conversion of energy and transfer of heat. Improving the effectiveness of solar energy
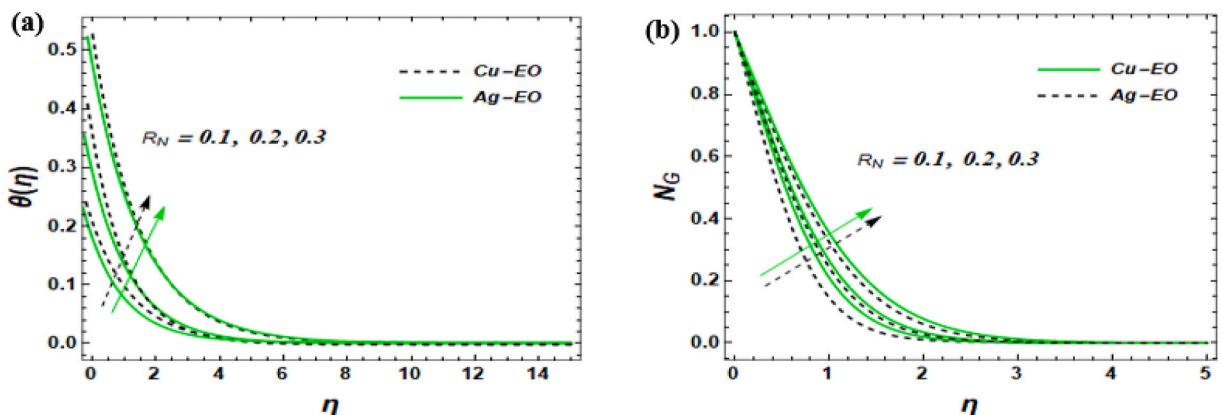

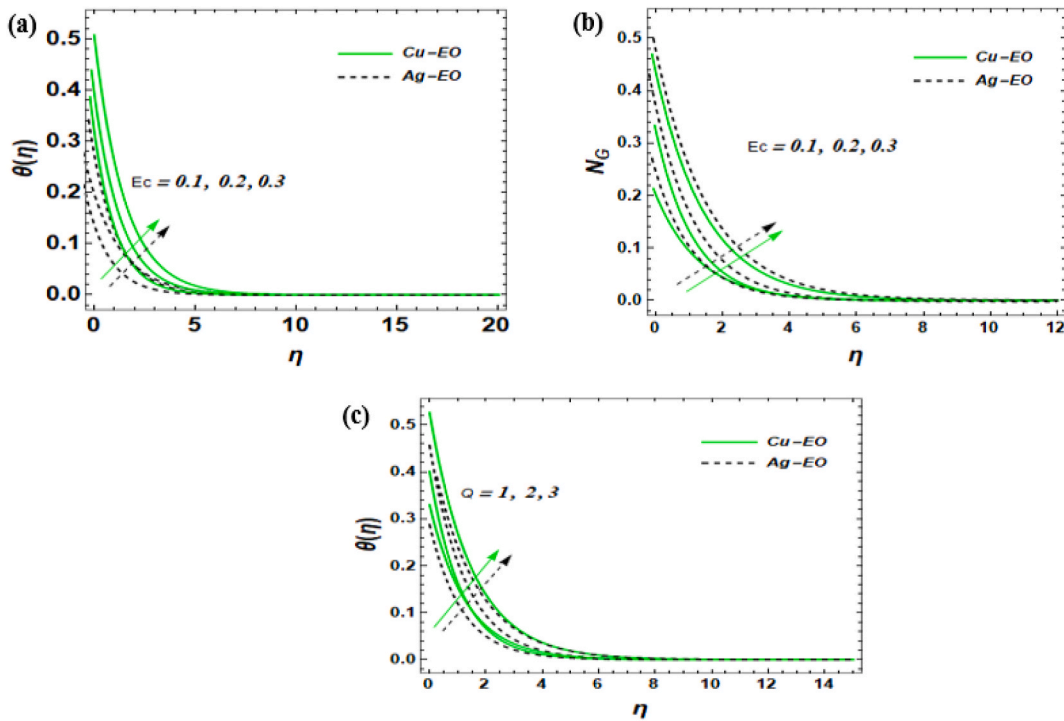**Fig. 7.** Impact of R_N and Q on $\theta(\eta)$ and N_G.

Fig. 8. Impact of *Ec and Q* on $\theta(\eta)$ and N_G.

systems can enhance their strength of this system (see Fig. 8).

6.5. Effect of Eckert number (Ec) and heat generation (Q) on thermal $\theta(\eta)$, and entropy generation (N_G) for (Cu-Engine oil) and (Ag − Engine oil) nanofluid

The has a great influence on temperature distribution. The Eckert number is a valuable parameter that can help describe the behavior of fluid flows that exhibit significant thermal effects, such as those observed in heat transfer. It offers insights into the relative importance of thermal effects with the kinetic energy of the flow. A high Eckert number indicates that kinetic energy is the dominant factor, while a low Eckert number implies that thermal effects carry more weight. The enhanced thermal conductivity of a nanofluid can lead to more effective heat transfer when the fluid is utilized in a system for heat dissipation [16]. This is because the nanoparticles in the nanofluid have the potential to increase the fluid's thermal conductivity, enabling it to transfer heat more quickly and effectively. Heat dissipation is a major contributor to entropy creation in the system. The heat dissipation can cause an increase in the internal energy of the system, leading to an improvement in the system of entropy generation. Entropy is a measurement of the disorder or unpredictability that exists inside a system, and it tends to rise with any process that cannot be reversed [29]. Regarding the physical aspect, heat dissipation in a combustion engine can lead to heightened friction and turbulence, which can cause an increase in entropy generation. On the other hand, heat dissipation in a refrigeration system can reduce entropy generation by removing heat from the system. Also, higher heat generation parameters will lead to an elevated temperature field. This is because there is an increase in the rate at which heat is being produced inside the system, which causes the temperature profile to rise.

6.6. Effect of volume friction of nanoparticles (φ) on temperature $\theta(\eta)$, and entropy generation (N_G) for (Cu-Engine oil) and (Ag − Engine oil) nanofluid

The physical characteristics of a fluid, especially its fluid flow and thermal distribution, are greatly influenced by the presence of volume friction of nanoparticles in the fluid. Nanoparticles size effects are included as the primary factors in these five quantities, i.e.

$$\lambda_e = \frac{(k_s + (m-1)k_f) - (m-1)\varphi(k_f - k_s)}{(k_s + (m-1)k_f) + \varphi(k_f - k_s)}, \lambda_d = \left(1 + \frac{3\left(\frac{\sigma_s}{\sigma_f} - 1\right)\varphi}{\left(2 + \frac{\sigma_s}{\sigma_f}\right) - \left(\frac{\sigma_s}{\sigma_f} - 1\right)\varphi}\right), \lambda_c = \left((1 - \varphi) + \varphi \frac{(\rho C_p)_s}{(\rho C_p)_f}\right), \lambda_b = \left(1 - \varphi + \varphi\left(\frac{\rho_s}{\rho_f}\right)\right), \lambda_a = (1 - \varphi)^{2.5} \text{ based on}$$

the Tiwari-Das nanoscale model, which is stated in equation (19). Meanwhile, the effect of volume friction of nanoparticles reduces the velocity profile. In a physical view of point. viscosity refers to how much a fluid resists flowing. When adding nano molecules to a fluid, they can interact with the fluid molecules and create friction, which makes it harder for the fluid to flow. This can cause the fluid to become more viscous and slow down its flow rate. In addition, the nano molecule size contributes significantly to increasing the thermal distribution. The tiny size and larger surface area to volume ratio of nanoparticles can cause an increase in the thermal distribution. Due to the greater surface area that nanoparticles possess, when they are introduced into a system, they can absorb energy in a more effective way than larger particles. The transfer of absorbed energy from nanoparticles to the surrounding medium can cause

the thermal distribution to increase. Also, The amount at which chemical reactions occur can be accelerated by the use of nanoparticles as catalysts, which can raise the system's temperature. Furthermore, nanoparticles have a higher ability to absorb and emit radiation than larger particles, which may also influence temperature distribution. When nanofluids are subjected to solar radiation, the fluid's nanoparticles absorb the energy and elevate its temperature.

6.7. Effect of Biot number (B_i) on temperature $\theta(\eta)$, and entropy generation (N_G) for (Cu-Engine oil) and (Ag − Engine oil) nanofluid

Biot number is a ratio between the thermal resistance on the inside and the thermal resistance on the outside (see Fig. 9). The external resistance is mostly caused by heat transfer through convection. Therefore, rising values of the Biot number $B_i = \left(\frac{h_f}{k_o}\sqrt{\frac{v_f(1-\xi t)}{b}}\right)$ enhance the thermal field and causes an increase in the temperature distribution illustrated in Fig. 10a. Physically, when Bi is less than one ($Bi < 1$), the material of internal thermal resistance is substantially lower than its external thermal resistance [62]. However, this situation occurs frequently in systems in which conduction within a solid material dominates over convection or radiation at the surface. When the value of B_i is significantly higher than 1 ($B_i > 1$), the body experiences a much higher internal thermal resistance compared to its external thermal resistance. As a result, the system exhibits non-uniform temperature distribution. When Bi equals infinity ($B_i = \infty$), the body's internal thermal resistance is much lower than its external thermal resistance, leading to a uniform temperature distribution within the body. Also, when a substance is subjected to sunlight, it takes in a portion of the energy and transforms it into thermal energy. When a substance is exposed to solar radiation, it assimilates a certain amount of energy and changes it into thermal energy. the rate at which heat is transferred from a material to its surroundings is dependent on several elements. However, these factors include the convective heat transfer coefficient (h_f), the thermal conductivity of the material (k_o). The B_i have a significant impact on the generation of entropy in a system undergoing heat transfer. Systems with low B_i exhibit higher rates of entropy generation, while systems with high Biot numbers exhibit lower rates of entropy generation (see Fig. 10b.)

6.8. Influence of Reynolds number (R_e) and Brinkman number (B_r) on temperature $\theta(\eta)$, and entropy generation (N_G) for (Cu-Engine oil) and (Ag − Engine oil) nanofluid

The process of creating models to represent energy losses that cannot be recovered requires the consideration of entropy generation, and the primary aim of this research is to identify approaches to reduce the speed at which these losses occur. The Reynolds number (Re) can be described as the relationship between the forces that resist fluid flow and the forces that promote fluid flow. To accomplish this objective, it is necessary to recognize the elements that contribute to the escalation of entropy and subsequently devise methods to diminish the rate of its occurrence. Fig. 11a illustrates how an increase in the Reynolds number intensifies the impact of factors that contribute to entropy production. Furthermore, the Brinkmann number is a measure of viscous and thermal diffusion in the flow of a fluid. when a Brinkmann number that is low means that viscous diffusion is more significant, whereas a Brinkmann number

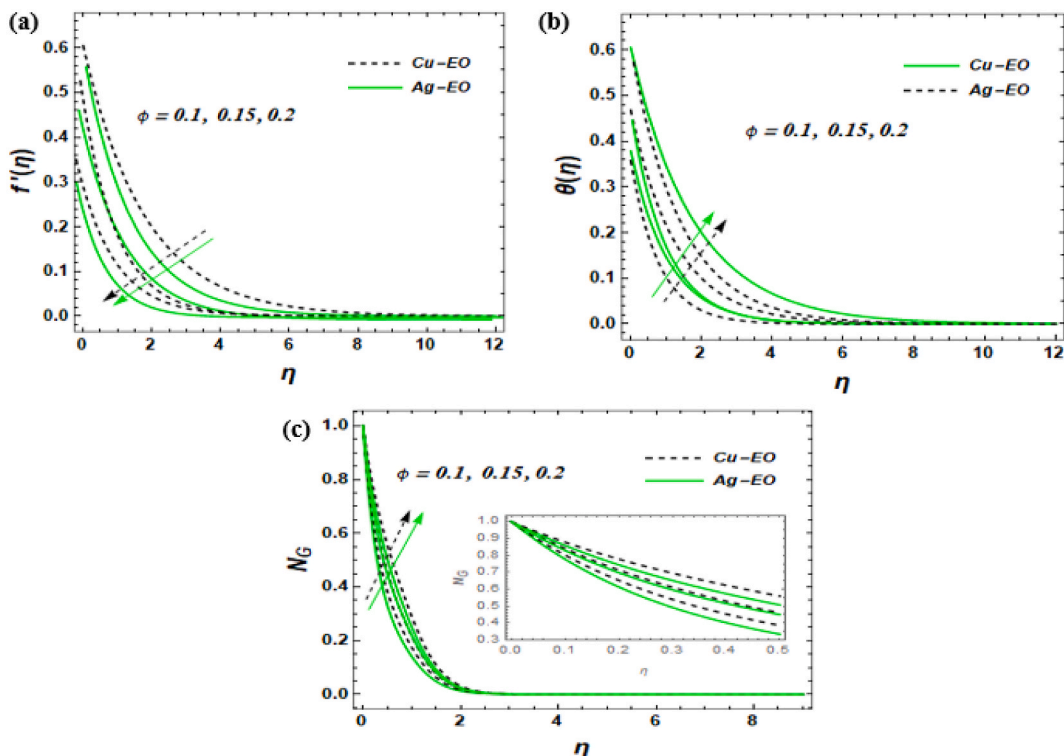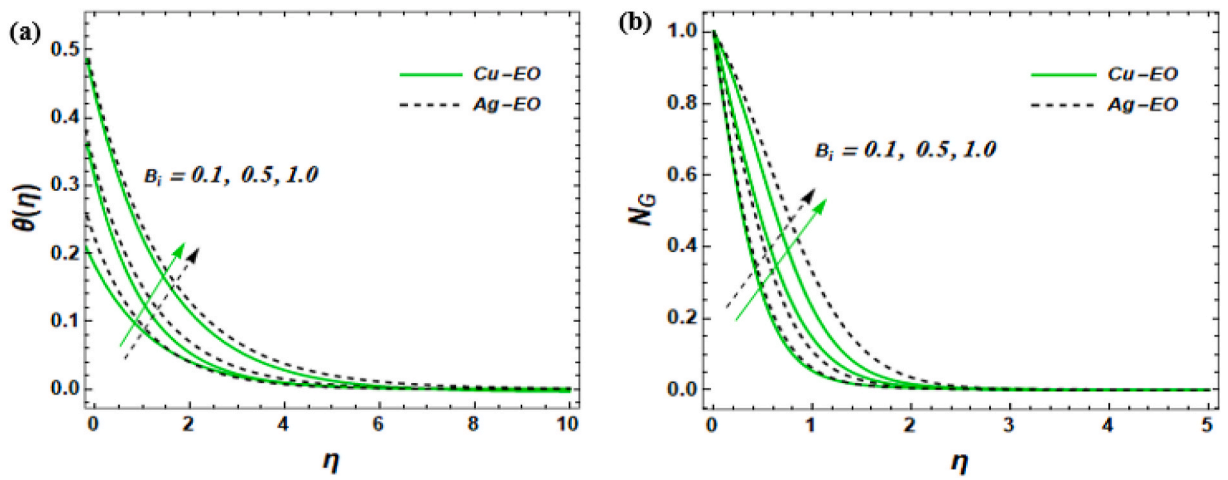**Fig. 9.** Impact of φ on $f'(\eta)$, $\theta(\eta)$, and (N_G)..

Fig. 10. Impact of B_i on $\theta(\eta)$, and (N_G)..
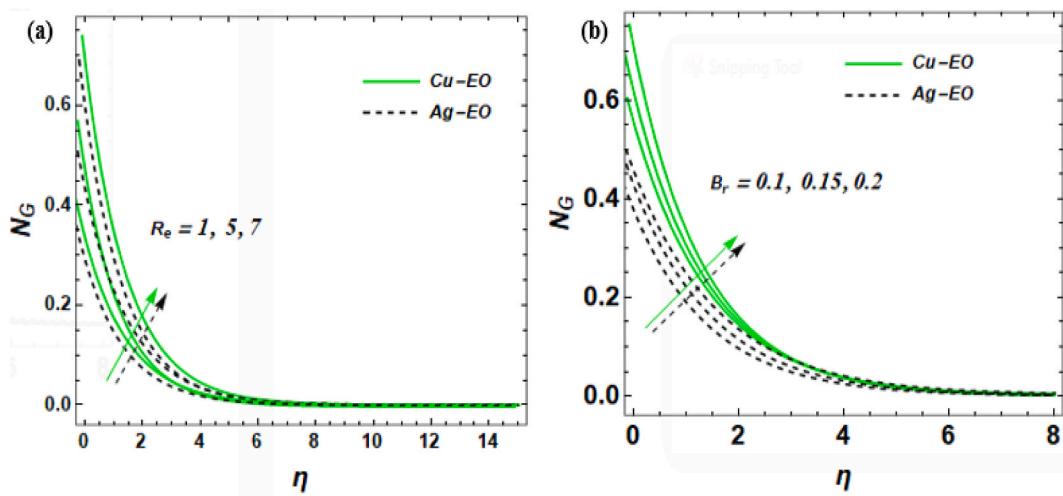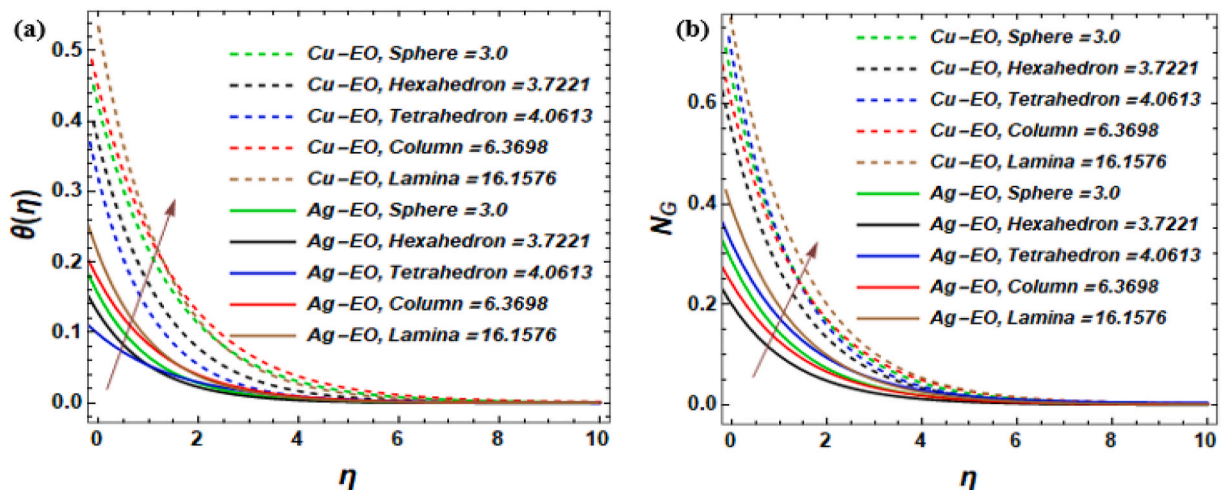

Fig. 11. Impact of B_i on $\theta(\eta)$, and (N_G)..

Fig. 12. Impact of m on $\theta(\eta)$, and (N_G)..

Table 3
Value of and wall heat gradient (Nu$_x$) for Pr=6450.

S	Nr	K_N	φ	$C_f Re_x^{1/2}$ Cu-Engine oil	$Ag-$ Engine oil	Nu_x Cu-Engine oil	$Ag-$ Engine oil
0.1				4.3542	2.1795	1.2682	0.1011
0.2				4.4674	2.3097	1.3754	0.1024
0.3				4.5321	2.5654	1.5028	0.1031
	0.2			4.2111	2.2523	1.4570	0.1210
	0.4			4.2111	2.2523	0.6498	0.1470
	0.6			4.2111	2.2523	0.7828	0.6230
		2		4.5678	2.2345	1.6321	0.4132
		4		4.6856	2.3912	1.5421	0.3564
		6		4.7421	2.5151	1.4652	0.1954
			0.1	4.6990	2.3205	1.1651	0.1746
			0.15	4.0826	2.4020	1.1780	0.1604
			0.2	2.1466	1.5843	0.1882	0.1599

that is high indicates that thermal diffusion is more significant. However, The significance of the Brinkman number in the generation of entropy can be represented through a graph, where a dimensionless rate of N_G is plotted against the Brinkman number (B_r). This plot displays the entropy generation rate, which is standardized by the Reynolds number (Re) squared and is exhibited as a function of the Brinkman number. Reynolds number is another vital dimensionless factor in fluid mechanics, which determines the ratio of viscous forces to inertial forces. The upcoming figure shows that the rate at which dimensionless entropy is formed increases steadily with the B_r, indicating that entropy generation also rises with the viscous dissipation of the system. Additionally, the plot indicates that at higher B_r, the rate of N_G accelerates, indicating that the importance of viscous dissipation grows as the flow becomes more viscous. This is supported by the observation that the rate of N_G increases rapidly as the Brinkman number increases.

6.9. Influence of shaped nanoparticles (tetrahedron, lamina column, sphere, and hexahedron) on temperature $\theta(\eta)$, andentropygeneration(N_G) for (Cu-Engine oil) and (Ag − Engine oil) nanofluid

Fig. 12 (a, and b) present an analysis and investigation of the impact of several parameters and the use of five differently shaped nanoparticles (tetrahedron, lamina column, sphere, and hexahedron) on temperature and entropy profiles. The illustration in Fig. 12 (a, and b) demonstrates the shape parameter (m) of nanoparticles' elevated temperature and entropy generation profile. It can be noticed that temperatures rise as the shape factor increases. This occurrence is because of the higher thermal conductivity. In addition, when compared to spheres, hexahedrons, tetrahedrons, and columns, lamina-shaped nanoparticles have been shown to generate a greater field temperature. Physically, lamina-shaped nanoparticles can be utilized to increase the efficiency of heat transfer in a wide range of applications, including heat exchangers, solar thermal systems, and electronics cooling. Due to the utilization of these nanoparticles, the thermal conductivity of the base fluid can be greatly improved, which leads to higher efficiency in heat transfer. In applications that involve the storage of energy, such as solar thermal systems and supercapacitors, lamina-shaped nanofluids may be utilized. The high surface area of these nanofluids can improve the electrochemical performance of the electrolyte and, as a result, the efficiency of devices that store energy. This can be achieved by boosting the active area on the surface of the electrode.

Table 3 presents information on how the drag coefficient (Cf), heat transfer rate (Nu_x) are affected by the controlled parameters of the flow. Table 3 displays an increase in drag coefficient and the rate of heat transmission when control variables are utilized. It has been observed that an increase in the quantity of permeability (K_N), nanomolecules size (φ) and suction (S) parameter leads to an enhancement of the drag coefficient. Additionally, it has been claimed that changes in thermal radiation (Nr) do not affect the drag coefficient for Cu-EO and Ag-EO nanoparticles as the parameters increase. The current method's accuracy was checked by comparing the heat transfer rate values of the problem with previously published results. Table 4 shows that there was a good agreement between them.

7. Conclusion

The study focuses on analyzing the behavior of $Ag-EO$ and $Cu-EO$ Williamson nanofluids within a parabolic trough solar collector, which is under the influence of thermal radiation fluxing, and magnetic fields. The analysis will consider the velocity flow, fluid temperature, and entropy production aspects in a thermally radiated environment. The infinite porous stretching surface is covered by the nanofluid. The mathematical model takes into account different factors such as the impact of heat source/sink, thermal radiation, slip condition, nanoparticles shape feature, and viscous dissipation in the region of the boundary layer. Moreover, the solutions derived from Chebyshev Collocation Spectral Method have been verified with the previous study, demonstrating complete conformity with the chosen parameters. Graphs and tables were used to visually represent the results, which were then analyzed. The analysis of the figures revealed certain important factors that were observed during the parametric studies, and these are listed below.

- The $Ag-EO$ Williamson nanofluids have a smoother flow compared to the $Cu-EO$ mixture fluid.
- The boundary layer experiences a higher rate of heat transfer when the shape factor m is smaller.
- When the volume fraction of nanoparticles is raised, the rate of heat transfer also increases.
- The boundary layer experiences the highest temperature when using particles with a lamina shape, while the lowest temperature is observed when using spherical-shaped nanoparticles.

Table 4

Comparison of heat transfer rate (Nu_x) for varying value of the Prandtl number (pr).

Pr	Present outcome	The outcomes of [63]	The outcomes of [64]	The outcomes of [65] new work	The outcomes of [66]
0.72	0.8086	0.80863135	0.80876122	0.8086	0.80876181
1.0	1.0000	1.00000000	1.00000000	1.0000	1.00000000
3.0	1.9237	1.92368259	1.92357431	1.9236	1.92357420
7.0	3.0723	3.07225021	3.07314679	3.0723	3.07314651
10	3.7207	3.72067390	3.72055436	3.7006	3.72055429

- The resistance to the movement of fluids was caused by various factors including the, WF parameter, Lorentz force, permeability parameter, nano molecules size, and slip parameter, which went against the natural flow.
- Apart from the factors mentioned earlier that create a favorable condition for thermal distribution, thermal radiation, and nanoparticles shape feature, magnetic, heat generation parameters also contribute to a better distribution of heat in the system.
- Controlling the irreversible loss of energy from a system can be achieved by utilizing various physical properties such as magnetic, permeability parameter, particle size and shape alteration, radiated heat, convective heat, Brinkman number, and Reynolds number. However, the slip parameter plays a significant role in reducing irreversibility.
- Interestingly, certain parameters have unique effects on the drag coefficient (Cf), heat transfer rate (Nu_x). The permeability related to porous media increases the skin friction but decreases the heat transfer rate (Nu_x) for $Ag - EO$ and $Cu - EO$ Williamson nanofluids. Another study found that parameters such as thermal radiation parameter positively influence the heat transfer rate (Nu_x).
- The numerical results indicated that adding a nanoparticles mixture of $Ag - EO$ and $Cu - EO$ to the fluid moving through the PTSC had dual benefits: it increased the heat transfer rate and generated a significant amount of energy.
- The Chebyshev Collocation Spectral Method (CCSM) produces a set of converging solutions for this problem, based on the physical parameter values used.

Future direction

In the near future, it is possible to test for various hybrid nano-fluid combinations to address specific heat transfer issues. This can be done by taking into account the surrounding physical conditions and addressing current industrial challenges that have not yet been resolved. The findings of this study could assist in enhancing the evaluation of heat impact from heating systems by considering non-Newtonian Prandtl-Eyring fluid. Furthermore, this approach could be broadened to incorporate temperature-dependent viscosity and chemical reaction. These advancements may lead to future improvements in the heating system design. The CCSM approach could be applied to a variety of physical and technical challenges in the future.

Author's contribution statement

A.M. Obalalu & C. Odetunde: Conceptualization, Methodology, Software, Validation; data curation; Formal analysis, Writing – original draft. **M. Asif Memon:** Writing–original draft, software, Investigation, Validation. **A. B. Shobo:** Writing–review & editing, Data curation, Visualization. **O. A Olayemi:** Validation, Investigation, Writing–review & editing, Formal analysis. **Mohamed R. Ali & R. Sadat:** Methodology, Formal analysis, Supervision, Funding. **M. M. Alqarni, Emad E. Mahmoud & A.S. Hendy:** provided significant feedback and assisted in the revised version of manuscript. Further, they have also assisted us in revising the manuscript critically for important intellectual content.

Declaration of competing interest

The authors declare that they have no known competing financial interests or personal relationships that could have appeared to influence the work reported in this paper.

Data availability

No data was used for the research described in the article.

References

[1] S. Salawu, A. Obalalu, E. Fatunmbi, R. Oderinu, Thermal Prandtl-Eyring hybridized MoS2-SiO2/C3H8O2 and SiO2-C3H8O2 nanofluids for effective solar energy absorber and entropy optimization: a solar water pump implementation, J. Mol. Liq. 361 (2022), 119608.

[2] S.M. Hussain, W. Jamshed, V. Kumar, V. Kumar, K.S. Nisar, M.R. Eid, R. Safdar, A.-H. Abdel-Aty, I. Yahia, Computational analysis of thermal energy distribution of electromagnetic Casson nanofluid across stretched sheet: shape factor effectiveness of solid-particles, Energy Rep. 7 (2021) 7460–7477.

[3] M.T. Kartal, The role of consumption of energy, fossil sources, nuclear energy, and renewable energy on environmental degradation in top-five carbon producing countries, Renew. Energy 184 (2022) 871–880.

[4] A. Kumar, P. Singh, P. Raizada, C.M. Hussain, Impact of COVID-19 on greenhouse gases emissions: a critical review, Sci. Total Environ. 806 (2022), 150349.

[5] M.H. Jahangir, M. Montazeri, S.A. Mousavi, A.J.R.E. Kargarzadeh, Reducing carbon emissions of industrial large livestock farms using hybrid, Renew. Ener. Sys. 189 (2022) 52–65.

[6] K. Zaman, A.R.A. Aziz, S. Sriyanto, Y. Indrianti, H. Jambari, The role of solar energy demand in the relationship between carbon pricing and environmental degradation: a blessing in disguise, J. Publ. Aff. 22 (2022), e2702.

[7] Y. Cai, G. Huang, S. Yeh, L. Liu, G. Li, A modeling approach for investigating climate change impacts on renewable energy utilization, Int. J. Energy Res. 36 (2012) 764–777.

[8] R.R. Barbosa, H.S. Schultz, L. da Costa Garcia, D.D. Martins, M. Carvalho, Economic and greenhouse gas assessments for two hot water industrial systems: solar vs. natural gas, Cleaner Eng. Technol. 6 (2022), 100365.

[9] A. Sacikumar, K. Adarsh, J. Singh, M. Indra, Development of solar powered evaporatively cooled tractor cab, AMA, Agricultural Mechanization in Asia, Africa and Latin America 49 (2018) 44–49.

[10] O.A. Olayemi, A.M. Obalalu, C.B. Odetunde, O.A. Ajala, Heat transfer enhancement of magnetized nanofluid flow due to a stretchable rotating disk with variable thermophysical properties effects, Eur. Physical J. Plus 137 (2022) 1–12.

[11] W. Jamshed, M.R. Eid, F. Shahzad, R. Safdar, M. Shamshuddin, Keller Box Analysis for Thermal Efficiency of Magneto Time-dependent Nanofluid Flowing in Solar-Powered Tractor Application Applying Nano-Metal Shaped Factor, Waves in Random Complex Media, 2022, pp. 1–36.

[12] A. Obalalu, T. Oreyeni, A. Abbas, M.A. Memon, U. Khan, E.-S.M. Sherif, A.M. Hassan, I. Pop, Implication of electromagnetohydrodynamic and heat transfer analysis in nanomaterial flow over a stretched surface: applications in solar energy, Case Stud. Therm. Eng. 49 (2023), 103381.

[13] S. Gorjian, H. Ebadi, M. Trommsdorff, H. Sharon, M. Demant, S. Schindele, The advent of modern solar-powered electric agricultural machinery: a solution for sustainable farm operations, J. Clean. Prod. 292 (2021), 126030.

[14] C.R. Gade, W.R. Sultana, Battery electric tractor powertrain component sizing with respect to energy consumption, driving patterns and performance evaluation using traction motor, Distr. Generat. Alternative Energy J. (2023), 789– 816.

[15] A.M. Obalalu, L.L. Adebayo, I. Colak, A.O. Ajala, F.A. Wahaab, Entropy generation minimization on electromagnetohydrodynamic radiative Casson nanofluid flow over a melting Riga plate, Heat Transfer 51 (5) (2022) 3951–3978.

[16] A.M. Obalalu, A.O. Ajala, A.O. Akindele, O.A. Oladapo, O.O. Akintayo, O.M. Jimoh, Computational study of magneto-convective non-Newtonian nanofluid slip flow over a stretching/shrinking sheet embedded in a porous medium, Comput. Math. Appl. 4 (2022) 123–128.

[17] A. Mahmood, A. Aziz, W. Jamshed, S. Hussain, Mathematical model for thermal solar collectors by using magnetohydrodynamic Maxwell nanofluid with slip conditions, thermal radiation and variable thermal conductivity, Results Phys. 7 (2017) 3425–3433.

[18] M.Y.A. Jamalabadi, J.H. Park, C.Y. Lee, Optimal Design of Magnetohydrodynamic Mixed Convection Flow in a Vertical Channel with Slip Boundary Conditions and Thermal Radiation Effects by Using an Entropy Generation Minimization Method, vol. 17, 2015, p. 866.

[19] S. Salawu, A. Obalalu, S. Okoya, Thermal convection and solar radiation of electromagnetic actuator Cu–Al2O3/C3H8O2 and Cu–C3H8O2 hybrid nanofluids for solar collector optimization, Mater. Today Commun. 33 (2022), 104763.

[20] S. Salawu, A. Obalalu, M. Shamshuddin, Nonlinear solar thermal radiation efficiency and energy optimization for magnetized hybrid Prandtl–eyring nanoliquid in aircraft, Arabian J. Sci. Eng. (2022) 1–12.

[21] N. Acharya, On the hydrothermal behavior and entropy analysis of buoyancy driven magnetohydrodynamic hybrid nanofluid flow within an octagonal enclosure fitted with fins: application to thermal energy storage, J. Energy Storage 53 (2022), 105198.

[22] N. Acharya, Spectral simulation on the flow patterns and thermal control of radiative nanofluid spraying on an inclined revolving disk considering the effect of nanoparticle diameter and solid–liquid interfacial layer, J. Heat Tran. 144 (2022), 092801.

[23] N. Acharya, S. Maity, P.K. Kundu, Entropy generation optimization of unsteady radiative hybrid nanofluid flow over a slippery spinning disk, Proc. IME C J. Mech. Eng. Sci. 236 (2022) 6007–6024.

[24] N. Acharya, Spectral simulation to investigate the effects of nanoparticle diameter and nanolayer on the ferrofluid flow over a slippery rotating disk in the presence of low oscillating magnetic field, Heat Transfer 50 (2021) 5951–5981.

[25] N. Acharya, Framing the impacts of highly oscillating magnetic field on the ferrofluid flow over a spinning disk considering nanoparticle diameter and solid–liquid interfacial layer, J. Heat Tran. 142 (2020), 102503.

[26] N. Acharya, Spectral quasi linearization simulation of radiative nanofluidic transport over a bended surface considering the effects of multiple convective conditions, Eur. J. Mech. B Fluid 84 (2020) 139–154.

[27] F. Shahzad, W. Jamshed, M.R. Eid, R.W. Ibrahim, R. Safdar, K.S. Nisar, M. Shamshuddin, Thermal Amelioration in Heat Transfer Rate Using Oldroyd-B Model Hybrid Nanofluid by CNTs-Based Kerosene Oil Flow in Solar Collectors Applications, Waves in Random Complex Media, 2022, pp. 1–31.

[28] F. Shahzad, J. Bouslimi, S. Gouadria, W. Jamshed, M.R. Eid, R. Safdar, M. Shamshuddin, K.S. Nisar, Hydrogen energy storage optimization in solar-HVAC using Sutterby nanofluid via Koo-Kleinstreuer and Li (KKL) correlations model: a solar thermal application, Int. J. Hydrogen Energy 47 (2022) 18877–18891.

[29] W. Jamshed, C. Şirin, F. Selimefendigil, Y. Altowairqi, M.R. Eid, Thermal characterization of coolant Maxwell type nanofluid flowing in parabolic trough solar collector (PTSC) used inside solar powered ship application, Coatings 11 (2021) 1552.

[30] S. Kuharat, O. Anwar Bég, A. Kadir, M. Shamshuddin, Computational study of heat transfer in solar collectors with different radiative flux models, Heat Tran. Asian Res. 48 (2019) 1002–1031.

[31] M. Shamshuddin, S. Salawu, F. Shahzad, W. Jamshed, M.R. Eid, G.R. Rajput, Thermal examination of chemical interaction and thermophoretic diffusion of Williamson fluid flow across Riga Plate surface with nonlinearity radiation flux, Numer. Heat Tran., Part A: Applications (2023) 1–15.

[32] A. Obalalu, M.A. Memon, O. Olayemi, J. Olilima, A. Fenta, Enhancing heat transfer in solar-powered ships: a study on hybrid nanofluids with carbon nanotubes and their application in parabolic trough solar collectors with electromagnetic controls, Sci. Rep. 13 (2023) 9476.

[33] P. Strohbeck, E. Eggenweiler, I. Rybak, A Modification of the Beavers–Joseph Condition for Arbitrary Flows to the Fluid–Porous Interface, Transport in Porous Media, 2023, pp. 1–24.

[34] A. Asghar, A.F. Chandio, Z. Shah, N. Vrinceanu, W. Deebani, M. Shutaywi, L.A. Lund, Magnetized mixed convection hybrid nanofluid with effect of heat generation/absorption and velocity slip condition, Heliyon 9 (2023).

[35] B. Kumbhakar, S. Nandi, Unsteady MHD radiative-dissipative flow of Cu-Al2O3/H2O hybrid nanofluid past a stretching sheet with slip and convective conditions: a regression analysis, Math. Comput. Simulat. 194 (2022) 563–587.

[36] A. Asghar, T.Y. Ying, K. Zaimi, Two-dimensional magnetized mixed convection hybrid nanofluid over a vertical exponentially shrinking sheet by thermal radiation, joule heating, velocity and thermal slip conditions, J. Adv. Res. Fluid Mech. Thermal Sci. 95 (2022) 159–179.

[37] U. Ali, M. Irfan, K.U. Rehman, A.S. Alqahtani, M. Malik, W. Shatanawi, On the Cattaneo– Christov Heat Flux Theory for Mixed Convection Flow Due to the Rotating Disk with Slip Effects, Waves in Random and Complex Media, 2022, pp. 1–15.

[38] A. Bejan, Fundamentals of exergy analysis, entropy generation minimization, and the generation of flow architecture, Int. J. Energy Res. 26 (2002).

[39] zA.M. Obalalu, A.O. Ajala, A.O. Akindele, O.A. Areo, S.D. Ogundiran, K.A. Salaudeen, S. Alao, Entropy Generation Minimization for Radiative Casson Fluid Flow through Permeable Walls and Convective Heating: A Comprehensive Numerical Investigation, Defect and Diffusion Forum, Trans Tech Publ, 2022, pp. 21–38.

[40] A. Obalalu, H. Ahmad, S. Salawu, O. Olayemi, C. Odetunde, A. Ajala, A. Abdulraheem, Improvement of Mechanical Energy Using Thermal Efficiency of Hybrid Nanofluid on Solar Aircraft Wings: an Application of Renewable, Sustainable Energy, Waves in Random Complex Media, 2023, pp. 1–30.

[41] F. Shahzad, W. Jamshed, M.R. Eid, R. Safdar, S.S. Putri Mohamed Isa, S.M. El Din, N.A.A. Mohd Nasir, A. Iqbal, Thermal cooling efficacy of a solar water pump using Oldroyd-B (aluminum alloy-titanium alloy/engine oil) hybrid nanofluid by applying new version for the model of Buongiorno, Sci. Rep. 12 (2022), 19817.

[42] H.A. Nabwey, F. Rahbar, T. Armaghani, A.M. Rashad, A.J. Chamkha, A comprehensive review of non-Newtonian nanofluid heat transfer, Symmetry 15 (2023) 362.

[43] R.V. Williamson, The flow of pseudoplastic materials, Ind. Eng. Chem. 21 (1929) 1108–1111.

[44] S.O. Salawu, A.M. Obalalu, E.I. Akinola, Current Density and Thermal Propagation of Electromagnetic CoFe2O4 and TiO2/C2H6O2+ H2O Hybridized Casson Nanofluids: A Concentrated Solar Power Maximization, 2023, 101200.

[45] A.M. Obalalu, O.A. Olayemi, C.B. Odetunde, O.A. Ajala, Significance of thermophoresis and Brownian motion on a reactive Casson Williamson nanofluid past a vertical moving cylinder, Comput. Therm. Sci.: Int. J. 15 (2023).

[46] K.A. Kumar, V. Sugunamma, N. Sandeep, J.R. Reddy, Numerical examination of MHD nonlinear radiative slip motion of non-Newtonian fluid across a stretching sheet in the presence of a porous medium, Heat Tran. Res. (2019) 50.

[47] M.I. Asjad, M. Zahid, M. Inc, D. Baleanu, B. Almohsen, Impact of activation energy and MHD on Williamson fluid flow in the presence of bioconvection, Alex. Eng. J. 61 (2022) 8715–8727.

[48] M. Hussain, A. Ali, M. Inc, N. Sene, M. Hussan, Impacts of chemical reaction and suction/injection on the mixed convective Williamson fluid past a penetrable porous wedge, J. Math. (2022) 2022.

[49] S. Sindhu, B. Gireesha, Scrutinization of unsteady non-Newtonian fluid flow considering buoyancy effect and thermal radiation: tangent hyperbolic model, Int. Commun. Heat mass transfer 135 (2022), 106062.

[50] A. Almaneea, Numerical study on heat and mass transport enhancement in MHD Williamson fluid via hybrid nanoparticles, Int. Commun. Heat mass transfer 61 (2022) 8343–8354.

[51] V.S. Patil, P.P. Humane, A.B. Patil, MHD Williamson nanofluid flow past a permeable stretching sheet with thermal radiation and chemical reaction, Int. J. Model. Simulat. (2022) 1–15.

[52] S.M. Hussain, W. Jamshed, V. Kumar, V. Kumar, K.S. Nisar, M.R. Eid, R. Safdar, A.-H. Abdel-Aty, I. Yahia, Computational analysis of thermal energy distribution of electromagnetic Casson nanofluid across stretched sheet: shape factor effectiveness of solid-particles, Energy Rep. 7 (2021) 7460–7477.

[53] S. Salawu, A. Obalalu, E. Fatunmbi, M. Shamshuddin, Elastic deformation of thermal radiative and convective hybrid SWCNT-Ag and MWCNT-MoS4 magneto-nanofluids flow in a cylinder, Results in Materials (2023), 100380.

[54] A.M. Obalalu, S.O. Salawu, O.A. Olayemi, O.A. Ajala, K. Issa, Analysis of hydromagnetic Williamson fluid flow over an inclined stretching sheet with Hall current using Galerkin Weighted Residual Method, Comput. Math. Appl. 146 (2023) 22–32.

[55] S. Salawu, A. Obalalu, E. Fatunmbi, A. Disu, N. Akkurt, Magneto-couple Stress of Tri- Hybrid Metallic Oxide Nanomaterials in Porous Media with Nonlinear Properties for Thermal Technology Advancement, Scientific African, 2023, e01841.

[56] Y. Lin, B. Li, L. Zheng, G.J.P.T. Chen, Particle Shape and Radiation Effects on Marangoni Boundary Layer Flow and Heat Transfer of Copper-Water Nanofluid Driven by an Exponential Temperature, vol. 301, 2016, pp. 379–386.

[57] U. Khan, A. Zaib, A. Ishak, S. Bakar, Time-dependent Blasius–Rayleigh–Stokes flow conveying hybrid nanofluid and heat transfer induced by non-fourier heat flux and transitive magnetic field, Case Stud. Therm. Eng. (2021), 101151.

[58] H. Ozawa, A. Ohmura, R.D. Lorenz, T. Pujol, The second law of thermodynamics and the global climate system: a review of the maximum entropy production principle, Rev. Geophys. 41 (2003).

[59] M.G. Reddy, M.S. Rani, M. Praveen, K.G. Kumar, Comparative study of different non- Newtonian fluid over an elaborated sheet in the view of dual stratified flow and ohmic heat, Chem. Phys. Lett. 784 (2021), 139096.

[60] A.M. Obalalu, Heat and mass transfer in an unsteady squeezed Casson fluid flow with novel thermophysical properties: analytical and numerical solution, Heat Transfer 50 (2021) 7988–8011.

[61] M.E. Nasr, M. Gnaneswara Reddy, W. Abbas, A.M. Megahed, E. Awwad, K.M. Khalil, Analysis of non-linear radiation and activation energy analysis on hydromagnetic reiner–Philippoff fluid flow with cattaneo–christov double diffusions, Mathematics 10 (2022) 1534.

[62] J. Wang, G. Tan, J. Wang, L.-F. Feng, Numerical study on flow, heat transfer and mixing of highly viscous non-Newtonian fluid in Sulzer mixer reactor, Int. J. Heat Mass Tran. 183 (2022), 122203.

[63] A. Ishak, R. Nazar, I. Pop, Mixed convection on the stagnation point flow toward a vertical, continuously stretching sheet, J. Heat Tran. (2007) 129.

[64] S. Das, S. Chakraborty, R. Jana, O. Makinde, Entropy analysis of unsteady magneto- nanofluid flow past accelerating stretching sheet with convective boundary condition 36 (2015) 1593–1610.

[65] A. Ishak, R. Nazar, I. Pop, Boundary layer flow and heat transfer over an unsteady stretching vertical surface, Meccanica 44 (2009) 369–375.

[66] W. Jamshed, S. Uma Devi S, R. Safdar, F. Redouane, K.S. Nisar, M.R. Eid, Comprehensive analysis on copper-iron (II, III)/oxide-engine oil Casson nanofluid flowing and thermal features in parabolic trough solar collector, J. Taibah Univ. Sci. 15 (2021) 619–636.